Tampere University

Lauri Puoskari

VARIABLE POWER TRANSFORMER WITH VOLTAGE AND PHASE SHIFT CONTROL

Master's Thesis
Faculty of Information Technology and Communication Sciences
Examiners: Paavo Rasilo
Amr Khadr
August 2025

ABSTRACT

Lauri Puoskari: Variable power transformer with voltage and phase shift control
Master's Thesis
Tampere University
Master's Programme in Electrical Engineering
August 2025

Voltage and phase shift control are essential in modern electric power systems. Traditionally voltage control has been implemented with power transformers equipped with on-load tap changers, and phase shift control with phase shifting transformers. These devices however have their own disadvantages such as mechanical fatigue and discrete step-wise operation. This thesis presents a novel power transformer design that can achieve continuous voltage and phase angle control by controlling the magentic flux inside the core structures of the transformer.

The transformer presented in this thesis utilizes the nonlinear magnetic characteristics of its core structures to control the magnetic flux paths in them. The core structures are saturated locally by feeding a direct current (DC) through auxiliary DC biasing windings, restricting the flow of magnetic flux through said part of the core. The goal of the transformer is to be able to produce an operating area of 0.9–1.1 p.u. secondary voltage and -60–60 ° phase shift.

The transformer was designed for a 50 Hz three-phase power system with 110 kV primary voltage and 20 kV secondary voltage. The transformer consists of three separate five-limbed cores for each primary phase with a coil on each limb. The primary coil of each phase is on the middle limb and to its left are the secondary coils of the same phase and to its right are the secondary coils of the next phase. The DC biasing windings are on both top and bottom yokes of the core structures between each limb.

An analytical model for the transformer was defined, and it was used for determining the appropriate numbers of turns for the coils. The resultant numbers of turns however did not produce the sought-after operating area, and the numbers of turns were therefore manually adjusted. The results of the analytical model were then used to determine the practical dimensions of the power transformer. A two-dimensional model with a mesh structure was then produced for finite element analysis (FEA).

Through static FEA, it was found that thin air gaps have to be added in the two limbs around the middle limb of the core structure to have the magnetic flux divide more evenly in the unsaturated scenario, since the voltages produced by the transformer without the air gaps were way too low for the intended operation. Through dynamic time-stepping FEA, it was in turn found that the voltage waveforms have increasing harmonic distortion with increasing absolute value of phase shift. The effect was smaller for the transformer without the air gaps, but still significant. The FEAs were carried out in no load conditions.

An operating area of 0.9–1.1 p.u. secondary voltage and -58–58 ° was achieved, which is fairly close to the original goal. The harmonic distortion in the secondary voltages, however, presents a new problem. In addition to reducing the harmonic distortion in the voltages, the transformer should also be tested in loaded conditions in the future.

Keywords: phase shift control, power transformer, transformer, variable transformer, virtual air gap, voltage control

TIIVISTELMÄ

Lauri Puoskari: Jännite- ja vaihesiirtosäädettävä tehomuuntaja
Diplomityö
Tampereen yliopisto
Sähkötekniikan DI-ohjelma
Elokuu 2025

Jännite- ja vaihesiirtosäätö ovat tärkeitä nykyisissä sähkövoimajärjestelmissä. Perinteisesti jännitesäätö on toteutettu käämikytkimillä varustetuilla tehomuuntajilla, ja vaihesiirtosäätö vaihesiirtomuuntajilla. Molemmilla laitteilla on kuitenkin omat haittansa, kuten mekaaninen rasitus ja portaittainen toiminta. Tämä työ tarjoaa uuden tehomuuntajamallin, jolla voidaan saada aikaan jatkuva jännite- ja vaihesiirtosäätö ohjaamalla sen rautasydämen sisäisen magneettivuon kulkureittejä.

Tässä työssä esitetty muuntaja hyödyntää rautasydämen epälineaarisia magneettisia ominaisuuksia ohjatakseen magneettivuon kulkureittejä. Rautasydän saturoidaan paikallisesti syöttämällä tasavirtaa apukäämeihin, mikä rajoittaa magneettivuon kulkua vastaavaa reittiä pitkin. Muuntajan tavoitteena on tuottaa 0.9–1.1 p.u. toisiojännitteen ja -60–60 ° vaihesiirron toiminta-alue.

Muuntaja suunniteltiin 50 Hz kolmivaihejärjestelmään 110 kV ensiöjännitteellä ja 20 kV toisiojännitteellä. Muuntaja koostuu kolmesta eri viisipylväisestä muuntajasydämestä, joiden joikaisessa pylväässä on yksi käämi. Ensiökäämit ovat jokaisen sydämen keskimmäisellä pylväällä, joiden vasemmalla puolella ovat saman vaiheen toisiokäämit ja oikealla puolella seuraavan vaiheen toisiokäämit. Apukäämit sijaitsevat sydämien ylä- ja alaikeissä, jokaisen pylvään välissä.

Muuntajalle määriteltiin analyyttinen malli, jota käytettiin sopivien käämien kierroslukujen selvittämiseen. Mallista saadut kierrosluvut eivät kuitenkaan saaneet aikaan tavoiteltua toiminta-aluetta, joten kierroslukuja säädettiin manuaalisesti. Analyyttisen mallin tuloksia käytettiin muuntajan käytännön mittojen selvittämiseen. Muuntajalle tuotettiin kaksiulotteinen malli verkkorakenteella elementtianalyysiä varten.

Staattisen elementtianalyysin kautta selvisi, että ohuet ilmavälit täytyy asettaa muuntajasydämien keskipylväiden viereisiin pylväisiin, jotta magneettivuo jakautuisi tasaisemmin eri pylväiden välille ilman saturaatiota, sillä ilman ilmavälejä muuntajan toisiojännitteet jäivät aivan liian alhaisiksi käyttökohteelle. Dynaamisen aika-askelluselementtianalyysin kautta selvisi, että toisiojännitteiden aaltomuodoissa ilmenee lisääntyvää harmonista säröä vaihesiirron itseisarvon kasvaessa. Ilmiö oli heikompi muuntajalla ilman ilmavälejä, mutta silti merkittävä. Elementtianalyysit tehtiin muuntajalle ilman kuormitusta.

0.9–1.1 p.u. toisiojännitteen ja -58–58 ° vaihesiirron toiminta-alue saavutettiin, joka on hyvin lähellä alkuperäistä tavoitetta. Harmoninen särö toisiojännitteissä kuitenkin tuo esiin uuden ongelman. Harmonisen särön vähentämisen lisäksi muuntaja tulisi tulevaisuudessa testata myös kuormituksen kanssa.

Avainsanat: jännitesäätö, muuntaja, säädettävä muuntaja, tehomuuntaja, vaihesiirtosäätö, virtuaalinen ilmaväli

USE OF ARTIFICIAL INTELLIGENCE IN THIS WORK

Artificial intelligence (AI) has been used in generating this work:

☒ No
☐ Yes

Acknowledgement of risks

I hereby acknowledge, that as the author of this work, I am fully responsible for the contents presented in this thesis. This includes the parts that were generated by an AI, in part or in their entirety. I therefore also acknowledge my responsibility in the case, where use of AI has resulted in ethical guidelines being breached.

PREFACE

This thesis was produced for Tampere University. I would like to thank my supervisors Paavo Rasilo and Amr Khadr for their help and guidance throughout the process of this thesis. I would also like to thank Paavo Rasilo for the unique opportunity to make this thesis about one of his inventions. Making this thesis was at times challenging but I'm all the more grateful for the experience.

Tampere, 15th August 2025

Lauri Puoskari

CONTENTS

LIST OF SYMBOLS

A	Surface area
$\boldsymbol{a}$	Nodal value vector of the magnetic vector potential
B, b	Magnetic flux density
$\boldsymbol{C}$	Coefficient matrix
$\boldsymbol{D}$	Coefficient matrix
d	Control signal value
E	Electromotive force
h	Linear height
I, i	Electrical current
J	Electrical current density
j	Imaginary unit
$\boldsymbol{K}$	Coefficient matrix
N	Number of turns
$\boldsymbol{Q}$	Coefficient matrix
R	Electrical resistance
S	Apparent power
$\boldsymbol{S}$	Stiffness matrix
t	Time
V, v	Voltage
w	Linear width
μ	Turns ratio
ϕ	Magnetic flux
ψ	Magnetic flux linkage
ω	Angular frequency

LIST OF ABBREVIATIONS

2D	Two-dimensional
DC	Direct current
EMF	Electromotive force
FEA	Finite element analysis
OLTC	On-load tap changer
PST	Phase-shifting transformer
THD	Total harmonic distortion

1. INTRODUCTION

Modern electric power networks are large and complex structures, which are subject to sudden and continuous operating point variations due to changes in generation, consumption and network topology. Even with these variations, the power networks still have to guarantee adequate load supply to its users. [1] It is therefore important that the voltage levels in the network are kept within acceptable limits.

In addition to voltage control, controlling the power flow between different points of the network is important, which is done by creating a difference in the magnitudes and/or the phase angles of their voltages [2]. Power flow control is needed, for example to prevent overloading in different branches of the power network, which is done by shifting some of the power flow through an alternative parallel path.

Traditionally, transformers equipped with on-load tap changers (OLTC) have been used as means to control voltage levels in the network, and phase-shifting transformers (PST) have been used as means to control power flows in the system [2], [3]. However, OLTCs are only capable of controlling the voltage in discrete steps, and since they are mechanical devices, they are susceptible to wear over time [4]. PSTs also require additional parts compared to traditional power transformers, which increase their costs [5].

This thesis aims to provide an alternative transformer design, that allows for continuous voltage and phase shift control without the use of moving mechanical parts like OLTCs. The control is instead implemented by controlling the magnetic flux paths inside the core structures of the transformer. The goal of the design is to allow for voltage control between 0.9–1.1 p.u. of the nominal secondary voltage and phase shift control between -60–60°.

In Chapter 2, the theoretical background for understanding the transformer is presented, after which the concept and design of the transformer are presented in Chapter 3. In Chapter 4, the analytical model of the transformer is presented, while the two-dimensional (2D) model of the transformer is presented in Chapter 5. In Chapter 6, static and dynamic finite element analyses (FEA) are carried out for the transformer and finally, the thesis is concluded in Chapter 7.

2. THEORETICAL BACKGROUND

In this chapter, the theoretical background for understanding the proposed transformer is presented. First, the basic electromagnetic theory relating to transformers is explained in Section 2.1 and then the characteristics of the power transformers and their traditional designs are explained in Section 2.2. In Section 2.3, variable inductors and transformers and their previous applications are introduced.

2.1 Basic theory of transformers

When an alternating current goes through a conductor, a circular alternating magnetic field is induced around it [2]. When this conductor is wound into a solenoid, each turn in the coil intensifies the overall magnetic field going through the coil further [6]. If another conductor or a coil is brought into the magnetic field, a voltage will be induced over it, which is the principle the theory of transformers is based on [2].

Transformers are devices that transfer energy between two or more disconnected circuits by means of a common magnetic field. In a traditional one-phase-transformer, two coils are wound around an iron or steel core, i.e. ferromagnetic core, since the permeabilities of iron and steel are typically more than 1000 times that of air. Using such core also ensures that most of the magnetic flux goes through the coils as intended. [2]

The iron and steel cores used in transformers have also nonlinear magnetizing characteristics [2], and a typical magnetization curve of such core is presented in Figure 2.1. As can be seen from Figure 5.2, when magnetizing a ferromagnetic core with an external magnetic field, the magnetic flux density inside the core first increases slowly up to point A, after which it increases rapidly up to point B, after which the increase slows down, until it stops almost completely at point C. At point C, the material is saturated, and increasing the external magnetic field won't have a significant effect on the flux density in the material. When saturated, the material behaves magnetically similarly to air. [6]

According to Faraday's law of induction, the electromotive forces (EMF) over the individual coils of the transformer can be defined as

$$E = -N\frac{\mathrm{d}\phi}{\mathrm{d}t} = -\frac{\mathrm{d}\psi}{\mathrm{d}t}, \tag{2.1}$$

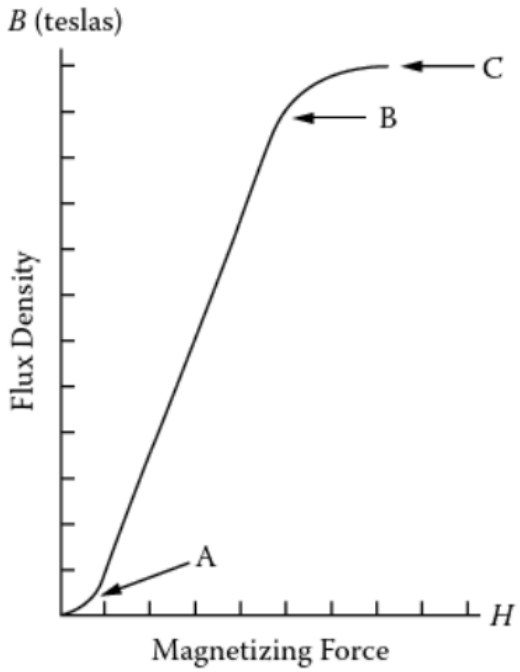

Figure 2.1. *Typical magnetization curve of a ferromagnetic core [6].*

where N is the number of turns in the coil, ϕ is the magnetic flux going through the coil and ψ is the magnetic flux linkage of the coil. When the same magnetic flux goes through both of the coils, the ratio of the EMFs is equal to the ratio of their numbers of turns

$$\frac{E_1}{E_2} = \frac{N_1}{N_2}, \tag{2.2}$$

which is how the transforming ratio is typically determined in traditional transformers.

If both the voltage and the magnetic flux are assumed sinusoidal, (2.1) can be expressed as

$$\hat{e} \sin \omega t = -N \frac{\mathrm{d}}{\mathrm{d}t} (\hat{\phi} \cos \omega t), \tag{2.3}$$

where $\hat{e}$ is the peak value of the EMF over the coil, ω is the angular frequency, t is the elapsed time and $\hat{\phi}$ is the peak value of the magnetic flux. According to (2.1), the voltage lags the magnetic flux by 90°. The sinusoidal waveform of the voltage can therefore be expressed as a sine function and the magnetic flux as a cosine function.

Since the magnetic flux can also be expressed as

$$\phi = BA, \tag{2.4}$$

where B is the magnetic flux density and A is the cross-sectional area of the magnetic

flux path, (2.3) can be expressed as

$$\hat{e}\sin\omega t = -N\frac{\mathrm{d}}{\mathrm{d}t}(\hat{b}A\cos\omega t), \tag{2.5}$$

where $\hat{b}$ is the peak value of the magnetic flux density. Equation (2.5) can then be further simplified into

$$\begin{aligned} \hat{e}\sin\omega t &= N\omega\hat{b}A\sin\omega t \\ \Rightarrow \hat{e} &= N\omega\hat{b}A, \end{aligned} \tag{2.6}$$

which can be used to determine the different parameters in the coil.

2.2 Power transformers

Power transformers are transformers, which transform a system of alternating voltage and current into another system, with different voltage and current levels, for the purpose of transmitting electrical power [7]. In other words, power transformers are used in different points of transmission and distribution networks to change the voltage and current levels according to the needs of the system.

Typical three-phase power transformers have a steel core with three limbs that are connected with yokes on both top and bottom sides. The windings of each phase are typically wound on their own limbs, with the primary and secondary windings on the same limb, one wound on top of the other. A schematic of such transformer is presented in Figure 2.2. [2]

The cores of power transformers are typically built out of thin, electrically insulated steel sheets, which are either stacked or wound together. The cross-sections of the cores can either be rectangular or circular, with the rectangular cross-sections usually used in smaller power transformers. [2]

The windings of the cores are typically made out of copper or aluminum, with copper being the more popular choice due to its more favorable characteristics. In transformers with voltage class of 25 kV and above, disc windings are mostly used. Disc windings consist of multiple discs that are stacked on top of each other and have either single or multiple insulated strands wound on top of each other. In Figure 2.3, a practical disc winding is presented. [2]

The voltage control of the transformers has traditionally been done with an OLTC, which is a mechanical device, that adjusts the turns ratio of the transformer by tapping a part of the winding in or out of the circuit, in discrete steps. However, the mechanical components of the OLTC, e.g. contacts, can experience wear over time, even though stronger materials and improved designs are used. [4] In the past, traditional OLTCs have also been too slow to deal with stability-related issues in the power system [8].

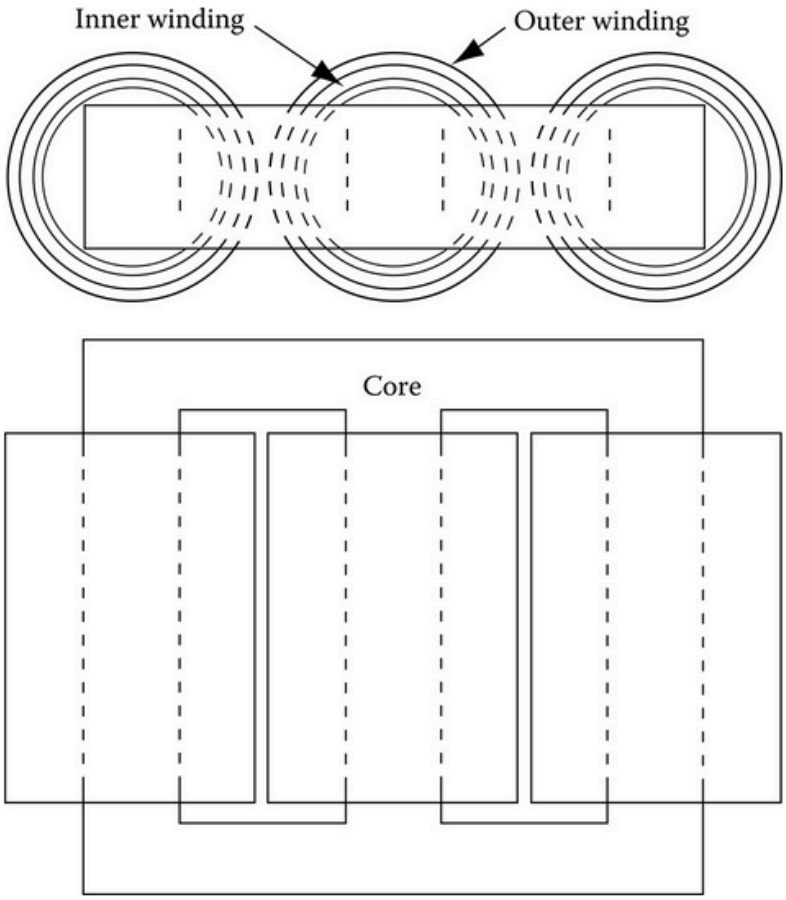

Figure 2.2. *A schematic of the structure of a typical three-phase power transformer [2].*

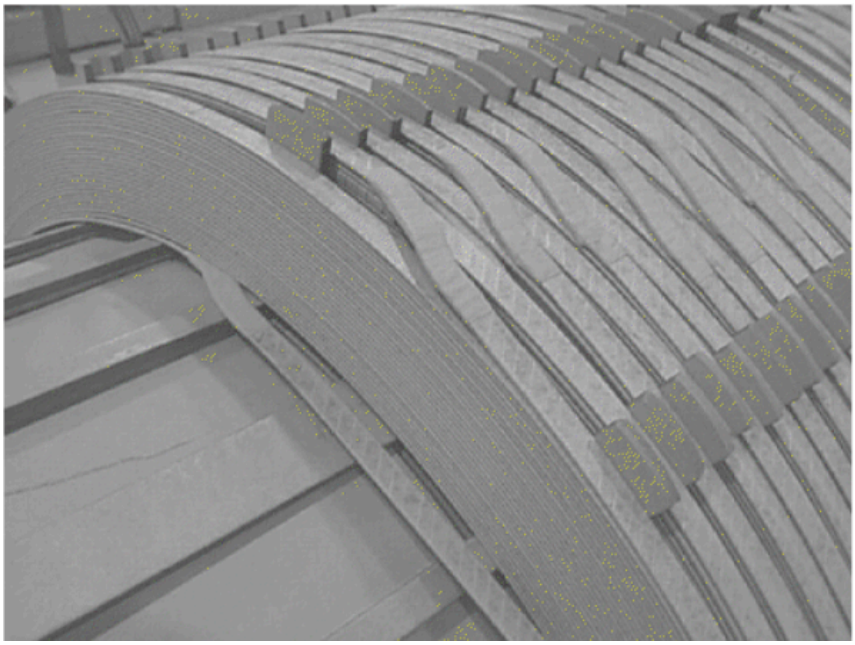

Figure 2.3. *A practical disc winding [2].*

PSTs are power transformers, that can alter the phase shift between the primary and secondary voltages of the transformer. In PSTs the phase shift is typically controlled by creating a controllable quadrature voltage, and injecting it into the secondary voltage, changing its apparent phase angle. However, compared to regular power transformers, PSTs require additional parts, e.g. tap changers or sometimes even an additional auxiliary transformer, which increase their costs. [5]

Power transformers are typically rated by their apparent power output, which can range from 500 kVA to over 100 MVA [2]. In three-phase power transformers the nominal power rating can be defined as

$$S_{\mathrm{n}} = \sqrt{3} V_{\mathrm{n}} I_{\mathrm{n}}, \tag{2.7}$$

where V_{n} is the nominal line-to-line voltage and I_{n} is the nominal line current of the transformer. Since the voltage level depends on the system that the transformer is designed to and typically remains constant, the increase in power rating usually leads to higher currents, and therefore larger windings and larger overall size of the transformer.

2.3 Variable inductors and transformers

Transformers and inductors, which use magnetization and saturation of their ferromagnetic core as means to control their behavior and properties, have been used in different applications before. The core of the transformer or inductor is typically equipped with one or more auxiliary windings, which are used to saturate the core locally by feeding a current through them. The saturation in the core affects the magnetic flux and its path in the core, resulting in variation in the magnetic properties and behavior of the device.

Variable inductors have been studied and used mainly in power electronics, in applications such as different power converters, electronic ballasts and maximum power point tracking in photovoltaic systems [9], [10], [11]. Variable inductors have also been studied and used in different power network applications, such as reactive power compensation and fault current limiting devices [12], [13].

Variable transformers have also been mainly studied and used in power electronics, in applications such as power converters, electronic ballasts and switched mode power supplies [14], [15], [16]. The use of variable transformers in power networks is also suggested by Dolan and Lehn [17], in order to control the voltage levels in the network. In addition to voltage control, the transformer proposed in this thesis would allow for phase shift control as well.

3. TRANSFORMER CONCEPT

In this chapter, the design and the operating principle of the proposed transformer are presented. In Section 3.1, the design and the structure of the proposed transformer are presented and explained, and in Section 3.2, the operation of the transformer is also explained.

3.1 Design concept

The transformer was designed for a traditional 50 Hz three-phase power network, with a primary voltage of 110 kV and secondary voltage of 20 kV and both primary and secondary sides in star connection. It was designed for functioning as the primary substation transformer of a 20 kV distribution network. In theory, the transformer should be able to operate between 0.9 and 1.1 p.u. secondary voltage and between -60 and 60 ° phase shift. The power rating of the transformer was decided to be 20 MVA to limit its size. The cross-section of the core was also decided to be rectangular for the sake of simplicity and accuracy of the 2D model.

In order to control both the phase shift and the magnitude of the secondary voltage, three five-limbed cores for each primary phase were designed. On the center of each core is the primary coil, to its left are two secondary coils of the same phase and to its right are two secondary coils of the next phase. One of the coils in the secondary coil pairs is used for controlling the phase shift, and the other for controlling the magnitude of the voltage. All four secondary coils of each phase are connected in series. The design of the transformer is presented in Figure 3.1.

Between each limb, on both the top and bottom yokes of the transformer, are direct current (DC) biasing coils, which are used to control the route of the magnetic flux in the core. Each coil is placed in four apertures in the transformer core, with each aperture having a current flowing to the opposite direction compared to its adjacent apertures, similarly to the double air gap windings presented in [18].

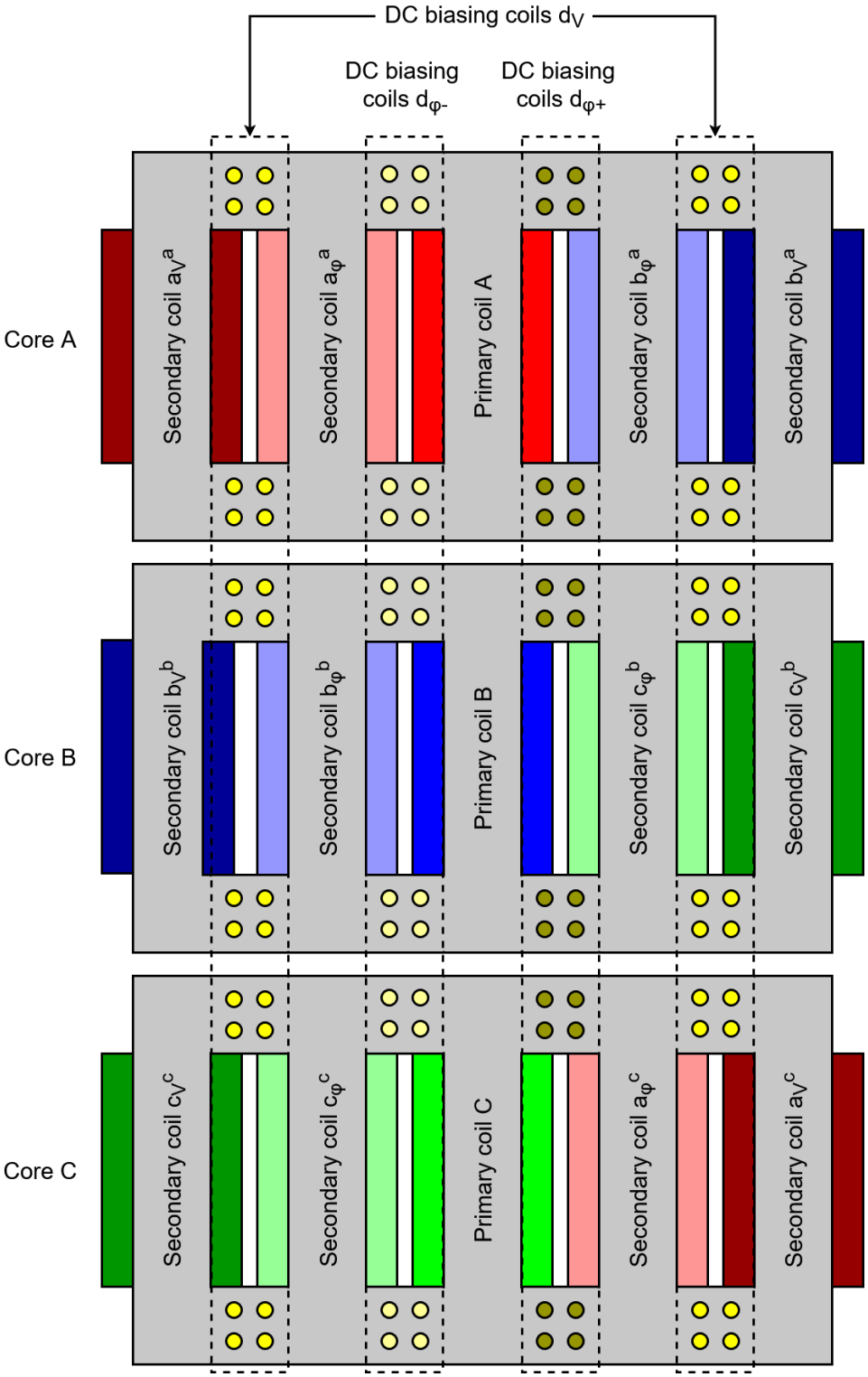

Figure 3.1. *Design of the proposed variable power transformer.*

The corresponding DC biasing coils in each core are connected in series, so that the transformer behaves symmetrically. The outermost DC biasing coils on the same core are also connected in series, so that both of the outermost secondary windings are excluded out of the magnetic circuit simultaneously. The innermost DC biasing coils are operated together in a way that they cannot both be fully saturated at the same time, so that the magnetic flux isn't forced out of the core.

3.2 Operating principle

The voltage and phase shift control of the transformer is done by managing the route of the magnetic flux in the core. The magnetic flux is prevented from going through a limb by saturating the core locally by feeding a current through the DC biasing coils. This creates a so-called virtual air gap, and the magnetic flux will adjust to path of least reluctance [18]. The apparent length of the virtual air gap can also be controlled by controlling the current flowing through the DC biasing winding.

The outermost secondary coils have a larger number of turns compared to the innermost secondary coils. By directing more of the flux through the outermost coils, the apparent overall number of turns in the secondary side of the transformer will become larger. As can be seen from (2.6), increasing the number of turns directly increases the EMF over the coil. Directing the magnetic flux through the outermost coils therefore increases the magnitude of the secondary voltage.

When no saturation is applied, the magnetic flux will be divided between the four secondary limbs. This results in a 60° phase shift between the primary and secondary voltages and in the maximum magnitude of the secondary voltage. If the outermost limbs are then saturated, the magnitude of the secondary voltage will drop, resulting in the minimum magnitude of the secondary voltage, if fully saturated.

When the magnetic flux is directed to the left through the secondary coils of the same phase as the primary coil, the resulting phase shift between the primary and secondary voltages is 0°. If the unsaturated case is thought of as the default scenario, the phase shift can be considered as –60°. As in the previous case, the magnitude of the secondary voltage can still be controlled by saturating the outermost limb.

When the magnetic flux is directed to the right through the secondary coils of the next phase of the primary coil, the resulting phase shift between the primary and secondary voltages is 120°. When compared to the unsaturated scenario, the phase shift can be considered as 60°. As before, the magnitude of the secondary voltage can be controlled by saturating the outermost limb.

4. ANALYTICAL MODEL

In this chapter, an analytical model for the transformer is presented. In Section 4.1, the complex turns ratio of the transformer is defined, in Section 4.2, the initial values for the numbers of turns in the windings are calculated and in Section 4.3, the theoretical operating points of the transformer are calculated. The analytical model is used as a starting point for the practical design and further simulation of the transformer.

4.1 Turns ratio

Let's define two control signals d_ϕ and d_V. Both control signals can have values between zero and one, and they are defined so that

- when $d_\phi = 0$, all of the magnetic fluxes in the cores are directed left,
- when $d_\phi = 0.5$, the magnetic fluxes in the cores are directed evenly to both left and right,
- when $d_\phi = 1$, all of the magnetic fluxes in the cores are directed right,
- when $d_\mathrm{V} = 0$, the magnetic fluxes in the cores are prevented from going through the outermost limbs,
- and when $d_\mathrm{V} = 1$, the magnetic fluxes in the cores are allowed to go through the outermost limbs without restrictions.

These two control signals can now be used in further defining the analytical model.

The turns ratio of a transformer can be defined as

$$\vec{\boldsymbol{\mu}} = \begin{bmatrix} \vec{V}_\mathrm{x}/\vec{V}_\mathrm{X} \\ \vec{V}_\mathrm{y}/\vec{V}_\mathrm{Y} \\ \vec{V}_\mathrm{z}/\vec{V}_\mathrm{Z} \end{bmatrix} \tag{4.1}$$

where $\vec{\boldsymbol{V}}_\mathrm{X}$, $\vec{\boldsymbol{V}}_\mathrm{Y}$ and $\vec{\boldsymbol{V}}_\mathrm{Z}$ are each phase of the primary voltage and $\vec{\boldsymbol{V}}_\mathrm{x}$, $\vec{\boldsymbol{V}}_\mathrm{y}$ and $\vec{\boldsymbol{V}}_\mathrm{z}$ are each phase of the secondary voltage, which are all defined by (2.1). Since the transformer is assumed symmetrical, only one phase has to be considered and (4.1) can be simplified

into

$$\vec{\mu} = \frac{\vec{V}_{\mathrm{x}}}{\vec{V}_{\mathrm{X}}}, \tag{4.2}$$

where $\vec{V}_{\mathrm{X}}$ is the primary voltage and $\vec{V}_{\mathrm{x}}$ is the secondary voltage of phase X.

Since the voltages are assumed sinusoidal, the flux linkages can be assumed sinusoidal as well, and their time derivatives can be defined as

$$\frac{\mathrm{d}\psi(t)}{\mathrm{d}t} = \mathrm{Re}\{j\omega\vec{\psi}e^{j\omega t}\}, \tag{4.3}$$

where ω is the angular frequency of the voltages and flux linkages. Now the turns ratio can be defined as

$$\vec{\mu} = \frac{\vec{V}_{\mathrm{x}}}{\vec{V}_{\mathrm{X}}} = \frac{-j\omega\vec{\psi}_{\mathrm{x}}e^{j\omega t}}{-j\omega\vec{\psi}_{\mathrm{X}}e^{j\omega t}} = \frac{\vec{\psi}_{\mathrm{x}}}{\vec{\psi}_{\mathrm{X}}}, \tag{4.4}$$

i.e. as the ratio of the secondary and primary flux linkages.

The primary flux linkage is easily defined as it's determined only by the primary voltage, but the secondary flux linkage is trickier due to overall contribution in multiple cores. The secondary flux linkage can be defined as

$$\begin{aligned}\vec{\psi}_{\mathrm{x}} &= \vec{\phi}_{\mathrm{X}}(d_{\upphi}^{\mathrm{x}}N_{\upphi}^{\mathrm{x}} + d_{\mathrm{V}}^{\mathrm{x}}N_{\mathrm{V}}^{\mathrm{x}}) + \vec{\phi}_{\mathrm{Z}}(d_{\upphi}^{\mathrm{z}}N_{\upphi}^{\mathrm{z}} + d_{\mathrm{V}}^{\mathrm{z}}N_{\mathrm{V}}^{\mathrm{z}}) \\ &= \frac{\vec{\psi}_{\mathrm{X}}}{N_{\mathrm{X}}}(d_{\upphi}^{\mathrm{x}}N_{\upphi}^{\mathrm{x}} + d_{\mathrm{V}}^{\mathrm{x}}N_{\mathrm{V}}^{\mathrm{x}}) + \frac{\vec{\psi}_{\mathrm{Z}}}{N_{\mathrm{Z}}}(d_{\upphi}^{\mathrm{z}}N_{\upphi}^{\mathrm{z}} + d_{\mathrm{V}}^{\mathrm{z}}N_{\mathrm{V}}^{\mathrm{z}}),\end{aligned} \tag{4.5}$$

where $\vec{\phi}_{\mathrm{X}}$ and $\vec{\phi}_{\mathrm{Z}}$ are the magnetic fluxes in the cores of the primary phases X and Z, $d_{\upphi}^{\mathrm{x}}$ and $d_{\upphi}^{\mathrm{z}}$ are the angular control signals of the secondary phases x and z, $d_{\mathrm{V}}^{\mathrm{x}}$ and $d_{\mathrm{V}}^{\mathrm{z}}$ are the amplitude control signals of the secondary phases x and z, $N_{\upphi}^{\mathrm{x}}$ and $N_{\upphi}^{\mathrm{z}}$ are the numbers of turns in the innermost secondary coils of phases x and z and $N_{\mathrm{V}}^{\mathrm{x}}$ and $N_{\mathrm{V}}^{\mathrm{z}}$ are the numbers of turns in the outermost secondary coils of phases x and z.

Since the transformer is assumed to be symmetrical, the corresponding numbers of turns in each core are equal:

$$N_{\mathrm{A}} = N_{\mathrm{B}} = N_{\mathrm{C}} = N_1, \tag{4.6}$$

$$N_{\upphi}^{\mathrm{a}} = N_{\upphi}^{\mathrm{b}} = N_{\upphi}^{\mathrm{c}} = N_{\upphi}, \tag{4.7}$$

and

$$N_{\mathrm{V}}^{\mathrm{a}} = N_{\mathrm{V}}^{\mathrm{b}} = N_{\mathrm{V}}^{\mathrm{c}} = N_{\mathrm{V}}, \tag{4.8}$$

and the relation between the flux linkages of phases X and Z can be defined as

$$\vec{\psi}_{\mathrm{Z}} = \vec{\psi}_{\mathrm{X}} \cdot 1\angle 120^\circ. \tag{4.9}$$

The definition of the turns ratio $\vec{\mu}$ can now be simplified into

$$\begin{aligned}\vec{\mu} &= \frac{\frac{\vec{\psi}_\mathrm{X}}{N_1}(d_\phi^\mathrm{x} N_\phi + d_\mathrm{V}^\mathrm{x} N_\mathrm{V}) + \frac{\vec{\psi}_\mathrm{X} \cdot 1\angle 120^\circ}{N_1}(d_\phi^\mathrm{z} N_\phi + d_\mathrm{V}^\mathrm{z} N_\mathrm{V})}{\vec{\psi}_\mathrm{X}} \\ &= \frac{d_\phi^\mathrm{x} N_\phi + d_\mathrm{V}^\mathrm{x} N_\mathrm{V} + 1\angle 120^\circ \cdot (d_\phi^\mathrm{z} N_\phi + d_\mathrm{V}^\mathrm{z} N_\mathrm{V})}{N_1} \\ &= \frac{N_\phi(d_\phi^\mathrm{x} + d_\phi^\mathrm{z} \cdot 1\angle 120^\circ) + N_\mathrm{V}(d_\mathrm{V}^\mathrm{x} + d_\mathrm{V}^\mathrm{z} \cdot 1\angle 120^\circ)}{N_1}.\end{aligned} \tag{4.10}$$

As can be seen from (4.10), the turns ratio $\vec{\mu}$ depends not only on the numbers of turns in each coil, but also the operating point, which can be changed continuously.

4.2 Numbers of turns in windings

The primary number of turns can be solved from (2.6), and with a $\hat{b}$ of 1.7 T and A of 0.5 m · 0.5 m, it equals to

$$\begin{aligned}N_1 &= \frac{\sqrt{2} \cdot 110\,000\,\mathrm{V}}{2\pi \cdot 50\,\mathrm{Hz} \cdot 1.7\,\mathrm{T} \cdot 0.25\,\mathrm{m}^2} \\ &= 1\,165.115... \\ &\approx 1\,200.\end{aligned} \tag{4.11}$$

To define the numbers of turns in secondary coils N_ϕ and N_V, two operating points were picked: minimum and maximum voltage points with a 60 ° phase shift between the primary and secondary voltage, i.e. 0 ° phase shift compared to the unsaturated scenario.

In the minimum voltage point, no flux is allowed to pass through the outermost limbs of the transformer, and the flux is allowed to divide evenly between the innermost secondary limbs. Therefore, the control signals in this case have values of

$$d_\phi^\mathrm{x} = d_\phi^\mathrm{z} = \frac{1}{2} \tag{4.12}$$

and

$$d_\mathrm{V}^\mathrm{x} = d_\mathrm{V}^\mathrm{z} = 0. \tag{4.13}$$

Now the turns ratio $\vec{\mu}$ can be simplified into

$$\begin{aligned}\vec{\mu} &= \frac{N_\phi(\frac{1}{2} + \frac{1}{2}\angle 120^\circ)}{N_1} \\ &= \frac{N_\phi}{2N_1} \cdot 1\angle 60^\circ.\end{aligned} \tag{4.14}$$

The turns ratio $\vec{\mu}$ can also be defined as the ratio between the secondary and primary

voltages, which are known to be in this case

$$V_{\mathrm{X}} = 110\,000\,\mathrm{V} \tag{4.15}$$

and

$$\vec{V_{\mathrm{x}}} = 18\,000\,\mathrm{V}\angle 60^\circ. \tag{4.16}$$

The number of turns in the innermost secondary coils N_ϕ can now be solved:

$$\begin{aligned} \frac{N_\phi}{2N_1} \cdot 1\angle 60^\circ &= \frac{\vec{V_{\mathrm{x}}}}{V_{\mathrm{X}}} \\ \Leftrightarrow N_\phi &= \frac{2N_1\vec{V_{\mathrm{x}}}}{V_{\mathrm{X}} \cdot 1\angle 60^\circ} \\ &= \frac{2 \cdot 1\,200 \cdot 18\,000\,\mathrm{V}\angle 60^\circ}{110\,000\,\mathrm{V}\angle 60^\circ} \\ &= 392.727... \\ &\approx 390. \end{aligned} \tag{4.17}$$

In the maximum voltage point with 60 ° phase shift, the magnetic flux is allowed to divide between all the limbs evenly. Therefore all the control signals in this case have a value of

$$d_\phi^{\mathrm{x}} = d_\phi^{\mathrm{z}} = d_{\mathrm{V}}^{\mathrm{x}} = d_{\mathrm{V}}^{\mathrm{z}} = \frac{1}{4}. \tag{4.18}$$

Now the turns ratio $\vec{\mu}$ can be simplified into

$$\begin{aligned} \vec{\mu} &= \frac{N_\phi(\frac{1}{4} + \frac{1}{4}\angle 120^\circ) + N_{\mathrm{V}}(\frac{1}{4} + \frac{1}{4}\angle 120^\circ)}{N_1} \\ &= \frac{N_\phi + N_{\mathrm{V}}}{4N_1} \cdot 1\angle 60^\circ. \end{aligned} \tag{4.19}$$

While the primary voltage stays the same, the secondary voltage in this case is

$$\vec{V_{\mathrm{x}}} = 22\,000\,\mathrm{V}\angle 60^\circ. \tag{4.20}$$

The number of turns in the outermost secondary coils N_{V} can now be solved:

$$\begin{aligned} \frac{N_\phi + N_{\mathrm{V}}}{4N_1} \cdot 1\angle 60^\circ &= \frac{\vec{V_{\mathrm{x}}}}{V_{\mathrm{X}}} \\ N_{\mathrm{V}} &= \frac{4N_1\vec{V_{\mathrm{x}}}}{V_{\mathrm{X}}\angle 60^\circ} - N_\phi \\ &= \frac{4 \cdot 1\,200 \cdot 22\,000\,\mathrm{V}\angle 60^\circ}{110\,000\,\mathrm{V}\angle 60^\circ} - 390 \\ &= 570. \end{aligned} \tag{4.21}$$

With the initial values for the numbers of turns in the coils determined, the analytical model can be further developed.

4.3 Operating points

Using the parameters determined in the previous section, the secondary voltages in different operating points of the transformer were calculated. This was done by defining four variables x, y, z and w, that can each have values between zero and one. These variables express whether the magnetic flux is allowed to go through the DC biasing coils or not, with x representing the left outermost limb, y both of the left limbs, z both of the right limbs and w the right outermost limb. The variables are also dependent on each other:

$$x = w, \tag{4.22}$$

and

$$y + z = 1, \tag{4.23}$$

which mean that the outermost biasing coils are operated in unison and that the magnetic flux is always allowed to go either left, right or both so that the flux isn't forced out of the core. Now the four variables have been decreased into two, since w can be replaced with x and z with $1 - y$. The control signals of the transformer can now be defined as

$$d_{\mathrm{V}}^{\mathrm{x}} = \frac{xy}{2}, \tag{4.24}$$

$$d_{\phi}^{\mathrm{x}} = (1 - \frac{x}{2})y, \tag{4.25}$$

$$d_{\phi}^{\mathrm{z}} = (1 - \frac{x}{2})(1 - y), \tag{4.26}$$

and

$$d_{\mathrm{V}}^{\mathrm{z}} = \frac{x(1-y)}{2}. \tag{4.27}$$

Since the transformer is assumed to behave symmetrically, only one phase is considered, and since all the control signals are now dependent on only two variables, the whole operating area of the transformer can be expressed in phase shift vs. amplitude plane. The operating points of the transformer with the numbers of turns of $N_1 = 1200$, $N_{\phi} = 390$ and $N_{\mathrm{V}} = 570$ are presented in Figure 4.1. The red circles in the figure represent the operating points that were used when determining the numbers of turns in the coils in the previous section.

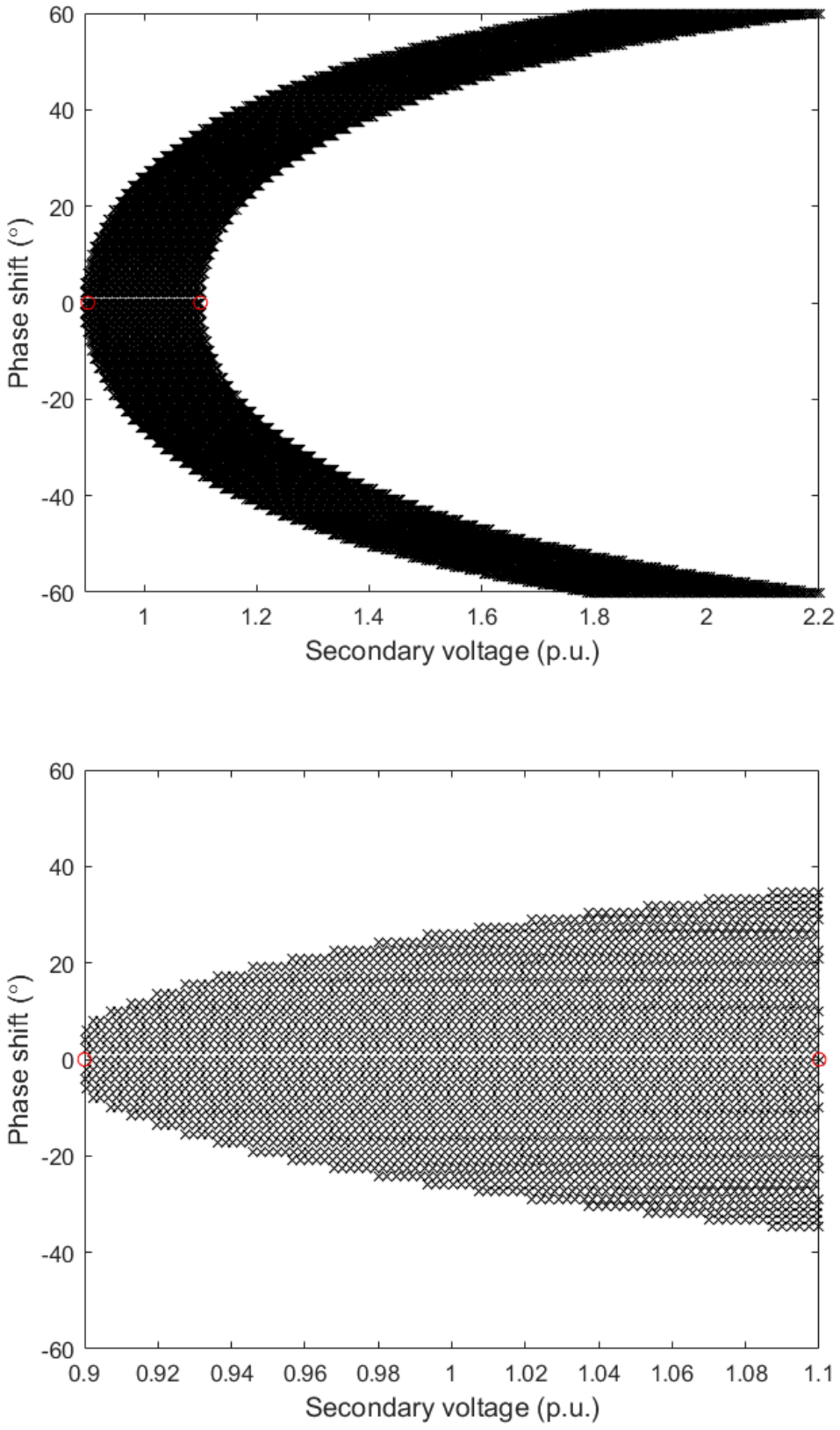

Figure 4.1. *Operating points of the transformer with* $N_1 = 1\,200$, $N_\phi = 390$ *and* $N_V = 570$.

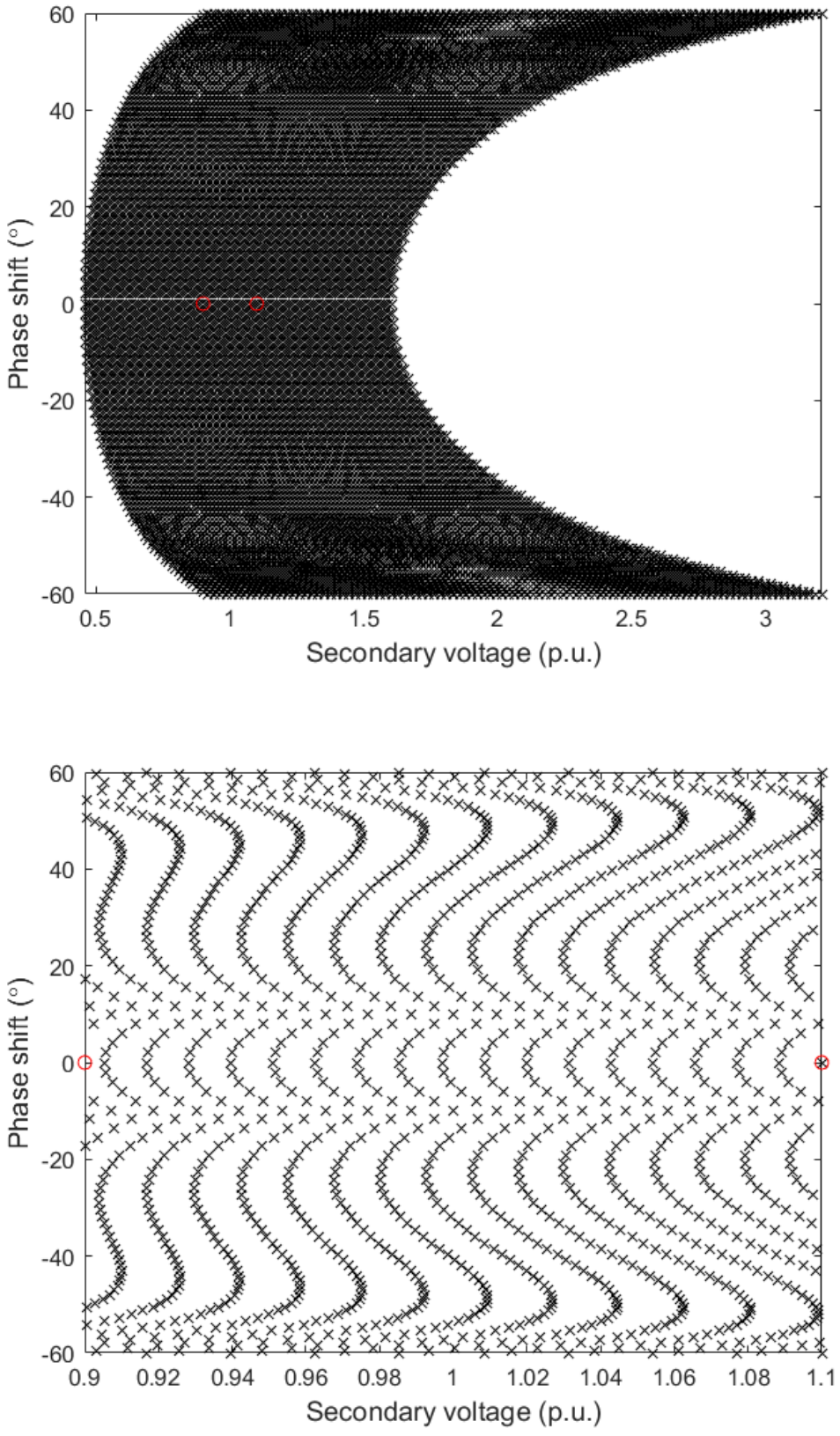

Figure 4.2. *Operating points of the transformer with* $N_1 = N_\mathrm{V} = 1\,200$ *and* $N_\Phi = 200$.

As can be seen from Figure 4.1, the operating points do not cover the whole theoretical operating area of 0.9–1.1 p.u. secondary voltage and -60–60 ° phase shift. By changing the numbers of turns in the transformer, the C-shaped area of operating points can be expanded to fit the whole theoretical operating area. The expanded area of operating points is presented in Figure 4.2, and it was achieved by decreasing N_ϕ to 200 and increasing N_V to 1 200.

As can be seen from Figure 4.2, the theoretical operating area is now filled entirely. The operating points are however no longer in a neat grid formation, but in a more warped formation, which could lead in difficulties when controlling the transformer. The outermost limbs are now also never fully but always partly saturated, which increases potential power losses.

5. 2D MODEL OF THE TRANSFORMER

In this chapter, the 2D model of the transformer is presented. In Section 5.1, the parameters for the practical design of the transformer are calculated, after which the design is presented. In Section 5.2, the 2D model of the transformer, which is later used for FEA, is presented.

5.1 Practical design

Using (2.7), the maximum currents of the transformer can be calculated. Since the power rating of the transformer is 20 MVA and the minimum operating secondary voltage is 0.9 p.u., the maximum primary and secondary currents of the transformer are

$$I_1 = \frac{S_\mathrm{n}}{\sqrt{3}V_1} = \frac{20\,\mathrm{MVA}}{\sqrt{3}\cdot 0.9\cdot 110\,\mathrm{kV}} = 116.636...\mathrm{A} \approx 117\,\mathrm{A}, \tag{5.1}$$

and

$$I_2 = \frac{S_\mathrm{n}}{\sqrt{3}V_2} = \frac{20\,\mathrm{MVA}}{\sqrt{3}\cdot 0.9\cdot 20\,\mathrm{kV}} = 641.500...\mathrm{A} \approx 642\,\mathrm{A}. \tag{5.2}$$

The maximum currents can now be used to define the minimum cross-sectional areas of the windings.

Since transformers of this size typically have disc windings, the maximum current density in the windings was set to be 3 A/mm^2, according to Zhu and Yang [19]. Now the required cross-sectional surface areas of the primary and secondary windings are

$$A_{\mathrm{w}1} = \frac{I_1}{J} = \frac{116.636...\mathrm{A}}{3\,\mathrm{A/mm^2}} = 38.878...\mathrm{mm}^2 \approx 39\mathrm{mm}^2, \tag{5.3}$$

and

$$A_{\mathrm{w}2} = \frac{I_2}{J} = \frac{641.600...\mathrm{A}}{3\,\mathrm{A/mm^2}} = 213.833...\mathrm{mm}^2 \approx 214\,\mathrm{mm}^2, \tag{5.4}$$

where J is the maximum current density in the windings.

Now since the numbers of turns and the cross-sectional areas of the windings are known, the areas taken up by the coils in the transformers can be calculated:

$$\begin{aligned} A_1 &= N_1 \cdot A_{\mathrm{w1}} \\ &= 1\,200 \cdot 38.878...\,\mathrm{mm}^2 \\ &= 46\,654.567...\,\mathrm{mm}^2 \\ &\approx 0.0467\,\mathrm{m}^2, \end{aligned} \tag{5.5}$$

$$\begin{aligned} A_\phi &= N_\phi \cdot A_{\mathrm{w2}} \\ &= 200 \cdot 213.833...\,\mathrm{mm}^2 \\ &= 42\,766.686...\,\mathrm{mm}^2 \\ &\approx 0.0428\,\mathrm{m}^2 \end{aligned} \tag{5.6}$$

and

$$\begin{aligned} A_{\mathrm{V}} &= N_{\mathrm{V}} \cdot A_{\mathrm{w2}} \\ &= 1\,200 \cdot 213.833...\,\mathrm{mm}^2 \\ &= 256\,600.119...\,\mathrm{mm}^2 \\ &\approx 0.257\,\mathrm{m}^2. \end{aligned} \tag{5.7}$$

The areas A_1, A_ϕ and A_{V} are taken up by the coils on both sides of the limbs, which means that their actual areas are twice as much.

The geometry of the transformer core was designed so that each limb's height is three times its width, and the space between each limb equals to the width of one limb. Since each limb was designed to be 0.5 m wide, their heights are therefore 1.5 m, and each coil have 0.25 m · 1.5 m of space between each limb. Assuming that the coils take up the entire height of each limb, the widths of the coil halves are

$$w_1 = \frac{A_1}{h} = \frac{46\,654.567...\,\mathrm{mm}^2}{1500\,\mathrm{mm}} = 31.103...\,\mathrm{mm} \approx 31.1\,\mathrm{mm}, \tag{5.8}$$

$$w_\phi = \frac{A_\phi}{h} = \frac{42\,766.686...\,\mathrm{mm}^2}{1500\,\mathrm{mm}} = 28.511...\,\mathrm{mm} \approx 28.5\,\mathrm{mm}, \tag{5.9}$$

and

$$w_{\mathrm{V}} = \frac{A_{\mathrm{V}}}{h} = \frac{256\,600.119...\,\mathrm{mm}^2}{1500\,\mathrm{mm}} = 171.066...\,\mathrm{mm} \approx 171.1\,\mathrm{mm}, \tag{5.10}$$

where h is the height of the limbs. As can be seen from (5.8)–(5.10), none of the widths of the coils exceed 250 mm, so none of them are too large for the core. The coils are connected in a way that the primary coils have current flowing in the opposite direction compared to the secondary coils.

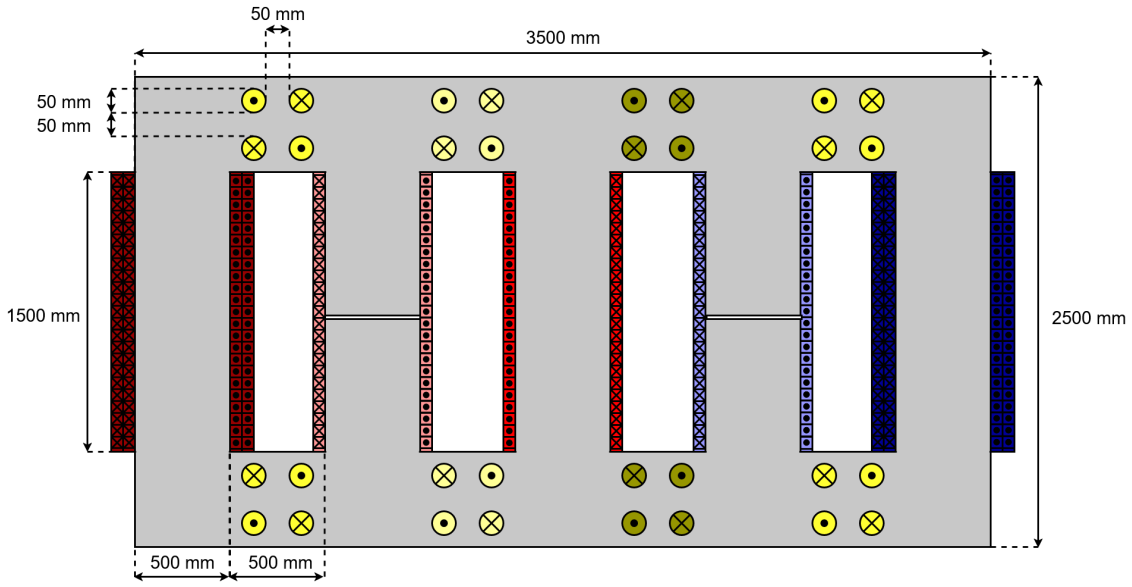

Figure 5.1. *The practical design of the transformer.*

The DC biasing coils are placed in circular apertures between each limb, so that each aperture has an equal amount of space between them. The apertures were chosen to have a diameter of 50 mm. The coils are connected so that on the top yoke, the top-left and bottom-right parts of the coils have currents flowing in positive z-direction and the top-right and bottom-left parts have currents flowing in negative z-direction. The maximum current flowing through the DC biasing coils was set to 20 A and the number of turns in each coil was set to 100. The practical design of the transformer is presented in Figure 5.1.

Since the magnetic flux paths to the outermost limbs are longer than those to the innermost secondary limbs, their magnetic reluctance is higher, and therefore the flux won't divide evenly between them and the innermost secondary limbs. This can be fixed by adding thin air gaps in the innermost secondary limbs, increasing their reluctance. The length of the air gap was considered as a variable when optimizing the operation of the transformer.

5.2 Model for finite element analysis

A 2D model based on the design in Figure 5.1 was created with COMSOL Multiphysics. The three cores are magnetically insulated from each other, and the cores are cut in half along the symmetry axis that goes through the middle of each limb to simplify the mesh. The mesh structure is presented in Figures 5.2 and 5.3.

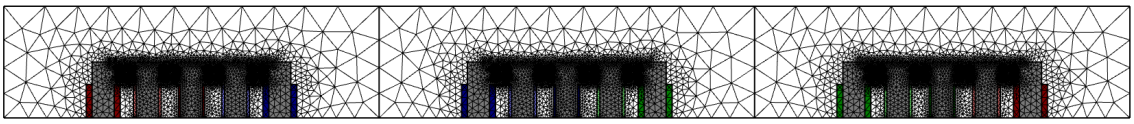

Figure 5.2. *The mesh structure of the whole transformer.*

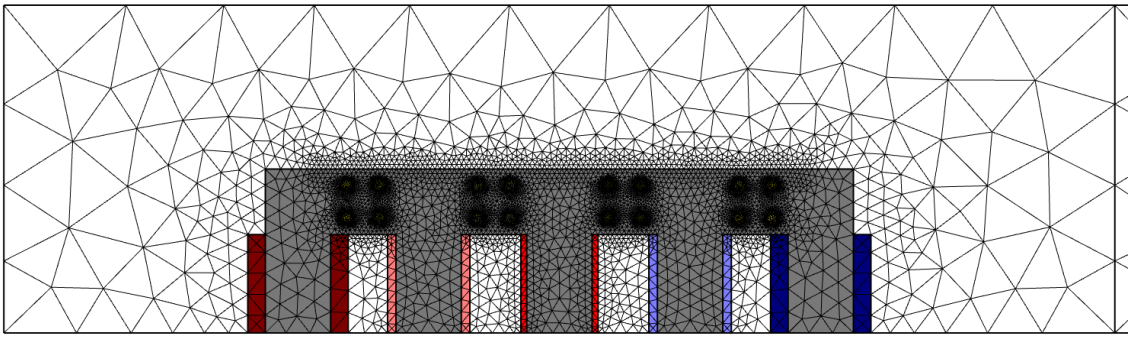

Figure 5.3. *The mesh structure of the core of phase A.*

The air gaps were excluded from the initial mesh structure to keep the number of elements to a minimum. Adding submillimetre air gaps into the cores increased the number of elements in the mesh fivefold, which increased the computation times significantly. The air gaps were added into the mesh structure in the MATLAB code used for handling the mesh structure. The method was later validated by comparing the results with both mesh structures.

6. FINITE ELEMENT ANALYSIS

In this chapter, the FEAs for the transformer are carried out. In Section 6.1, the finite element model of the transformer is defined. In Section 6.2, a static FEA is carried out for the transformer. Finally in section 6.3, a time-stepping FEA is carried out for the transformer.

6.1 Definition of the model

Since the primary side of the transformer is in a star connection with the star point disconnected from earth, the sum of the phase currents is always zero. Therefore only two of the three phase currents are independent on each other and matrices $\boldsymbol{K}$ and $\boldsymbol{Q}$ have to be defined for correcting the voltage and field equations of the model:

$$\boldsymbol{K} = \begin{bmatrix} 1 & 0 & -1 \\ 0 & 1 & -1 \end{bmatrix} \tag{6.1}$$

and

$$\boldsymbol{Q} = \begin{bmatrix} 0 & 0 & 1 \\ 1 & 0 & 1 \end{bmatrix}. \tag{6.2}$$

The matrices are then used in the field and voltage equations of the model with the primary voltages and currents, according to Arkkio [20].

The field equation of the model can be defined as

$$\begin{aligned} &\boldsymbol{S}(\boldsymbol{a})\boldsymbol{a} + \boldsymbol{C}_1 i_1 + \boldsymbol{C}_2 i_2 + \boldsymbol{C}_3 i_3 + ...\boldsymbol{C}_i i_i = 0 \\ \Leftrightarrow\ &\boldsymbol{S}(\boldsymbol{a})\boldsymbol{a} + \begin{bmatrix} \boldsymbol{C}_1 & \boldsymbol{C}_2 & \boldsymbol{C}_3 \end{bmatrix} \boldsymbol{K}^{\mathrm{T}} \begin{bmatrix} i_1 \\ i_2 \end{bmatrix} + \mathrm{C}_4 i_4 + ...\mathrm{C}_i i_i = 0, \end{aligned} \tag{6.3}$$

where $\boldsymbol{S}$ is the stiffness matrix, $\boldsymbol{a}$ is the nodal value vector of the magnetic vector potential, i_1–i_3 are the currents flowing in the primary coils, i_4–i_i are the currents flowing in the rest of the coils 4–i and $\boldsymbol{C}_1$–$\boldsymbol{C}_i$ are matrices that set the corresponding currents as sources in the field equation. Since no load was connected to the secondary side, secondary currents are defined zero.

The voltage equations of the coils are defined as

$$\boldsymbol{D}_i \frac{\mathrm{d}\boldsymbol{a}}{\mathrm{d}t} + R_i i_i - u_i = 0, \tag{6.4}$$

where $\boldsymbol{D}$ is a matrix that transforms vector potential $\boldsymbol{a}$ into magnetic flux, R_i is the resistance of coil i, i_i is the current flowing through coil i and u_i is the voltage across coil i. In the case of the primary voltages, the voltage equation is defined as

$$\boldsymbol{K}\boldsymbol{D}\frac{\mathrm{d}\boldsymbol{a}}{\mathrm{d}t} + R\boldsymbol{K}\boldsymbol{K}^{\mathrm{T}} \begin{bmatrix} i_1 \\ i_2 \end{bmatrix} - \boldsymbol{Q} \begin{bmatrix} u_{12} \\ u_{23} \\ u_{31} \end{bmatrix} = 0, \tag{6.5}$$

where u_{12}, u_{23} and u_{31} are the line-to-line primary voltages. The voltages over the inner- and outermost secondary coils are handled separately, and summed after. In the case of DC biasing coils, the currents are known, and the voltage equations aren't therefore needed. The resistances of the coils were set to 0.01 Ω.

6.2 Static finite element analysis

The static operation of the transformer without the air gaps was simulated in different operating points, which are presented in Figure 6.1. The x-axis represents the absolute value of the complex turns ratio $\vec{\mu}$ divided with the nominal turns ratio μ_{n}, which is 20/110 for this transformer. The y-axis represents the angle of the complex turns ratio $\vec{\mu}$. The x-axis is analogous to the relative magnitude of secondary voltage and the y-axis is analogous to the phase angle of the secondary voltage. The complex turns ratio is calculated from the phase flux linkages of the transformer instead of the voltages.

As can be seen from Figure 6.1, the absolute values of the complex turns ratio $\vec{\mu}$ are way too low for the intended operation, which makes the air gaps necessary for this model. It was found through manual testing that adding 0.5 mm air gaps in the innermost secondary limbs brings the voltages up to appropriate levels. The static operation of the transformer in different operating points was simulated again with the 0.5 mm air gaps implemented, and the results are presented in Figure 6.2.

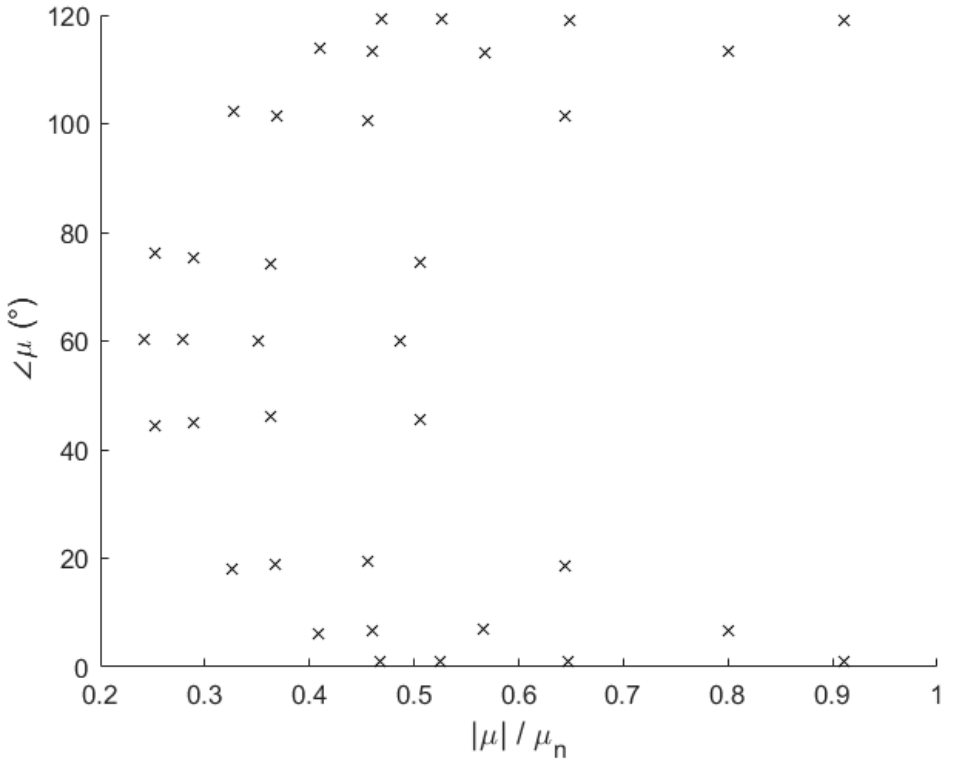

Figure 6.1. *The operating points of the transformer without the air gaps.*

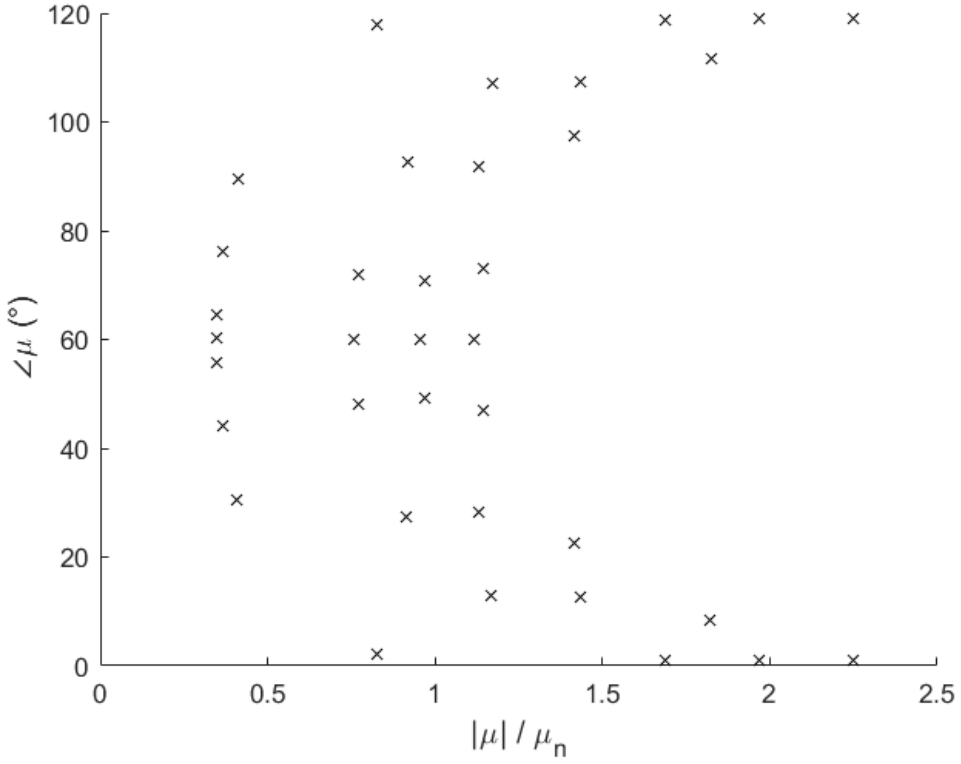

Figure 6.2. *The operating points of the transformer with the air gaps.*

As can be seen from Figures 6.1 and 6.2, the sensitivity of the controls varies greatly depending on the operating point. For example, slight change of current in phase shift control has much larger impact near 0.5 than 0 or 1. The operating points also fill the theoretical operating area almost entirely, so much optimization isn't necessary on that front. The used control signal values for the operating points in both cases were 0, 0.65, 0.8 and 1 for the voltage control and 0, 0.4, 0.44, 0.47, 0.5 0.53, 0.56, 0.6 and 1 for the phase angle control.

6.3 Time-stepping finite element analysis

The dynamic operation of the transformer was simulated for two fundamental periods using the time-stepping method. The operating points were chosen so that there are points for minimum, nominal and maximum voltage levels for every 10 ° phase shift. The currents in the DC biasing coils were ramped up from zero to the appropriate levels during the first period. The step-size was chosen so that there are 56 data points in each period.

The secondary voltage waveforms of the transformer with 0.5 mm air gaps are presented in Figures 6.3–6.9. The process was also repeated for the transformer without air gaps, the waveforms of which are presented in Figures 6.10-6.16. Since the transformer operated symmetrically with positive and negative phase shifts, only the waveforms with zero and negative phase shifts are presented here. In the figures, each phase has minimum, nominal and maximum waveforms, of which minimum waveform has the lowest amplitude, nominal waveform the second lowest amplitude and maximum waveform the highest amplitude.

As can be seen from Figures 6.3-6.9, the secondary voltage waveforms of the transformer seem to get increasingly harmonically distorted with increasing positive or decreasing negative phase shift. It seems that the harmonics have their phase shift independent of the angle of the fundamental waveform, since their peaks occur on different points of the fundamental waveform in each phase shift scenario.

As can be seen from Figures 6.10–6.16, with the transformer without the air gaps the waveforms seem smoother, but significant harmonics are still present, especially in –40 ° and –50 ° phase shift scenarios. As was demonstrated in the static analysis, the voltages are also too low for the intended operation of the transformer.

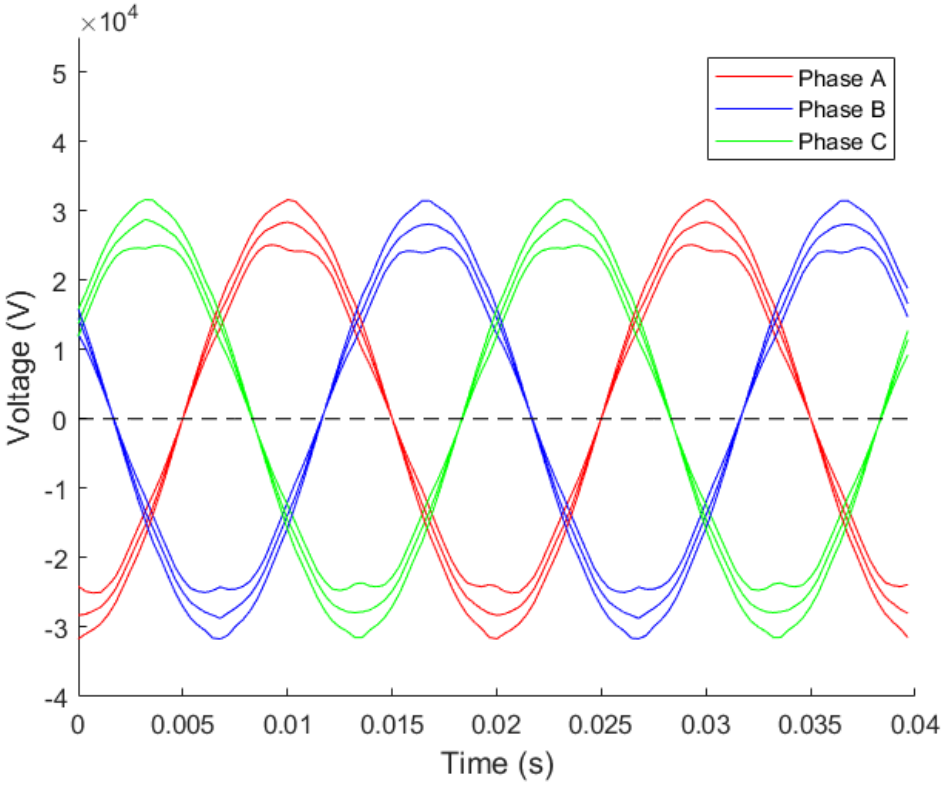

Figure 6.3. *Secondary voltage waveforms of the transformer with 0 ° phase shift.*

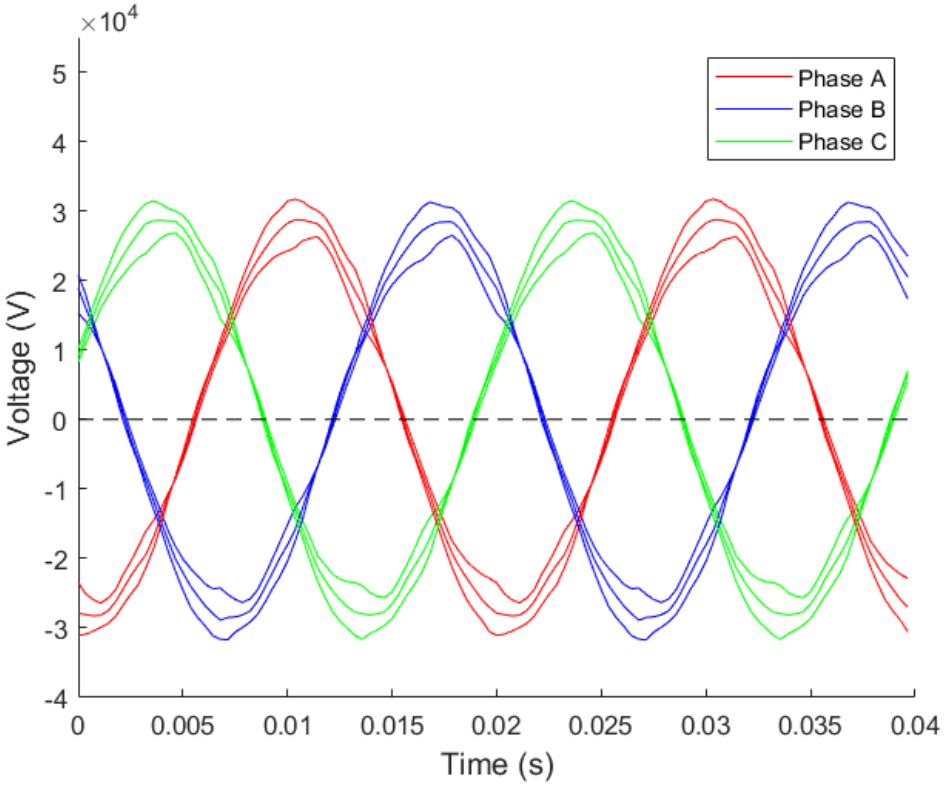

Figure 6.4. *Secondary voltage waveforms of the transformer with −10 ° phase shift.*

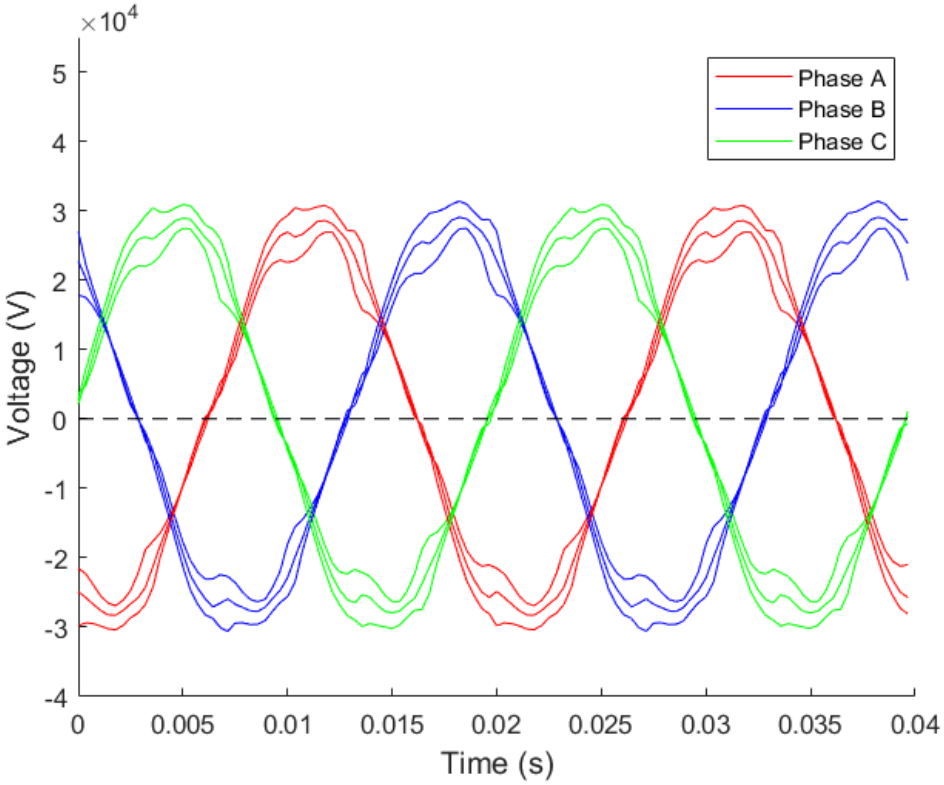

Figure 6.5. *Secondary voltage waveforms of the transformer with –20 ° phase shift.*

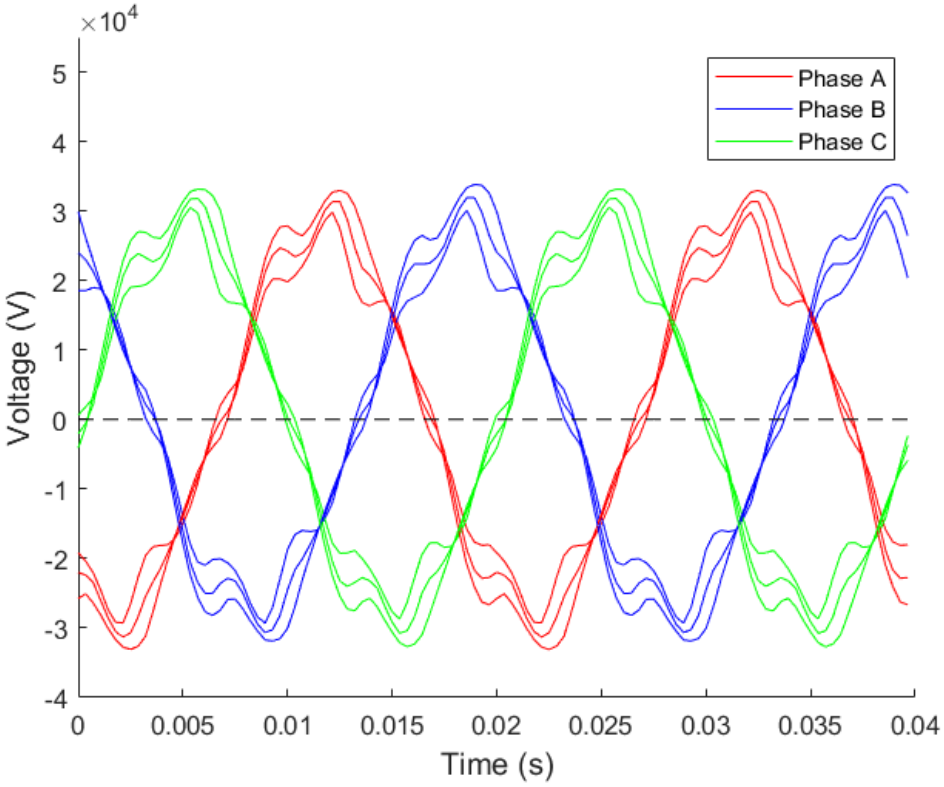

Figure 6.6. *Secondary voltage waveforms of the transformer with –30 ° phase shift.*

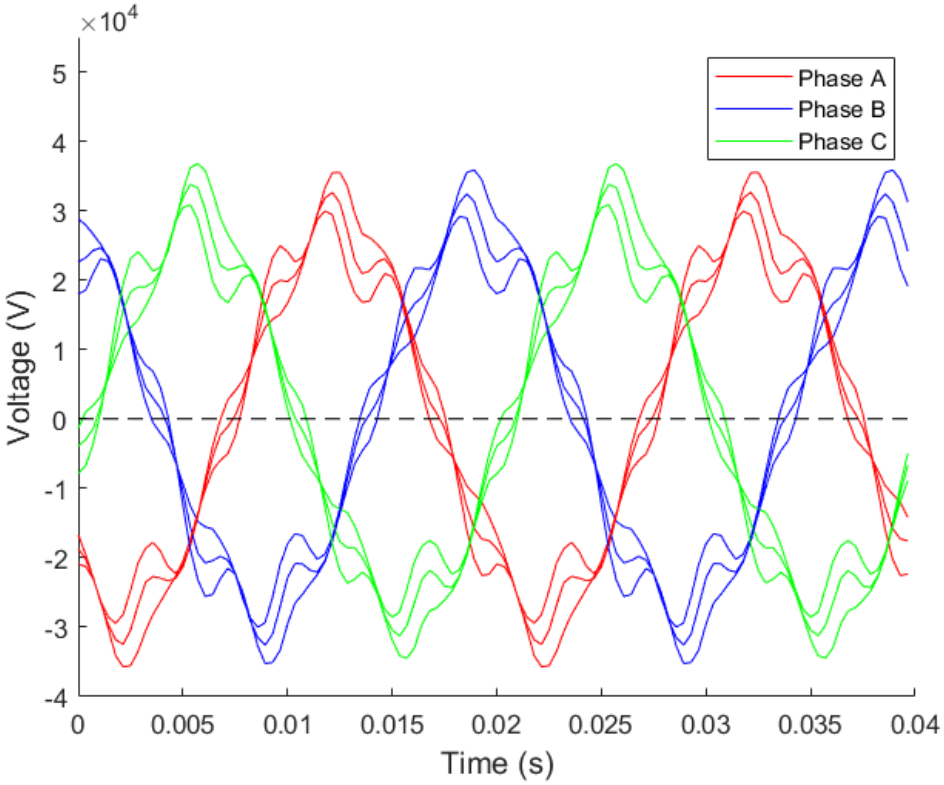

Figure 6.7. *Secondary voltage waveforms of the transformer with –40 ° phase shift.*

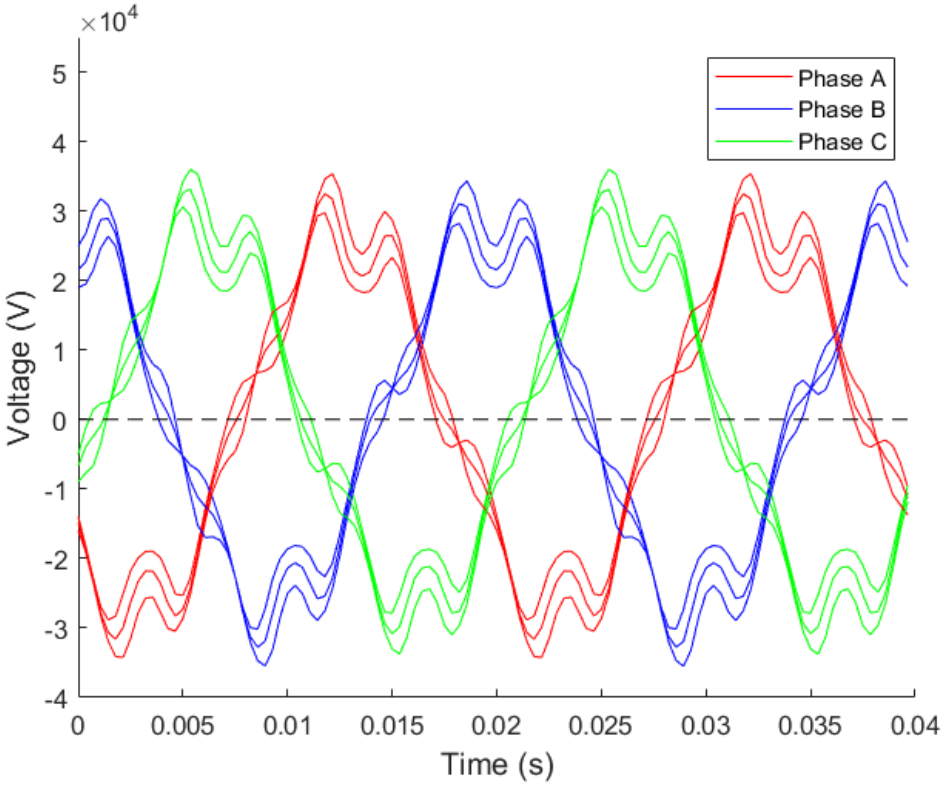

Figure 6.8. *Secondary voltage waveforms of the transformer with –50 ° phase shift.*

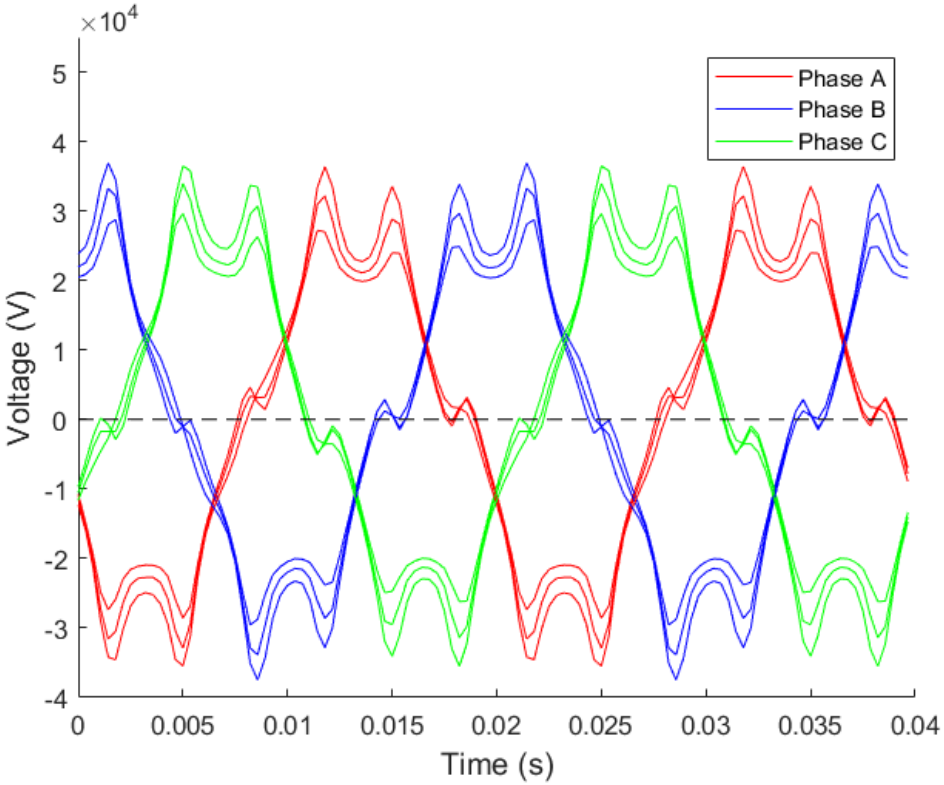

Figure 6.9. *Secondary voltage waveforms of the transformer with –58 ° phase shift.*

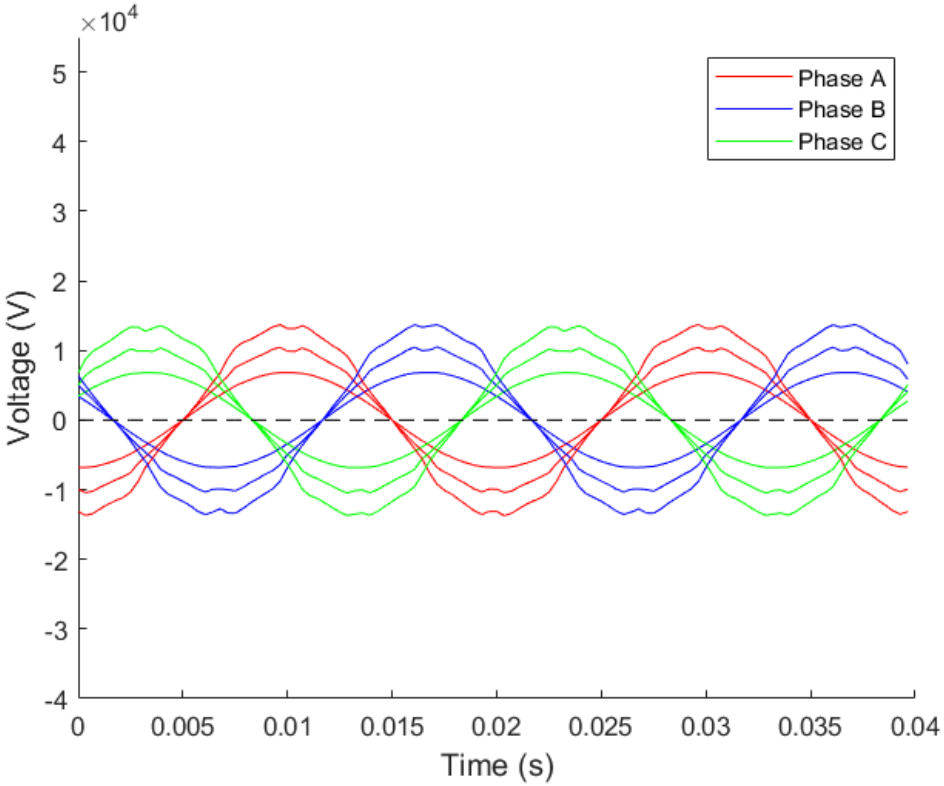

Figure 6.10. *Secondary voltage waveforms of the transformer without air gaps with 0 ° phase shift.*

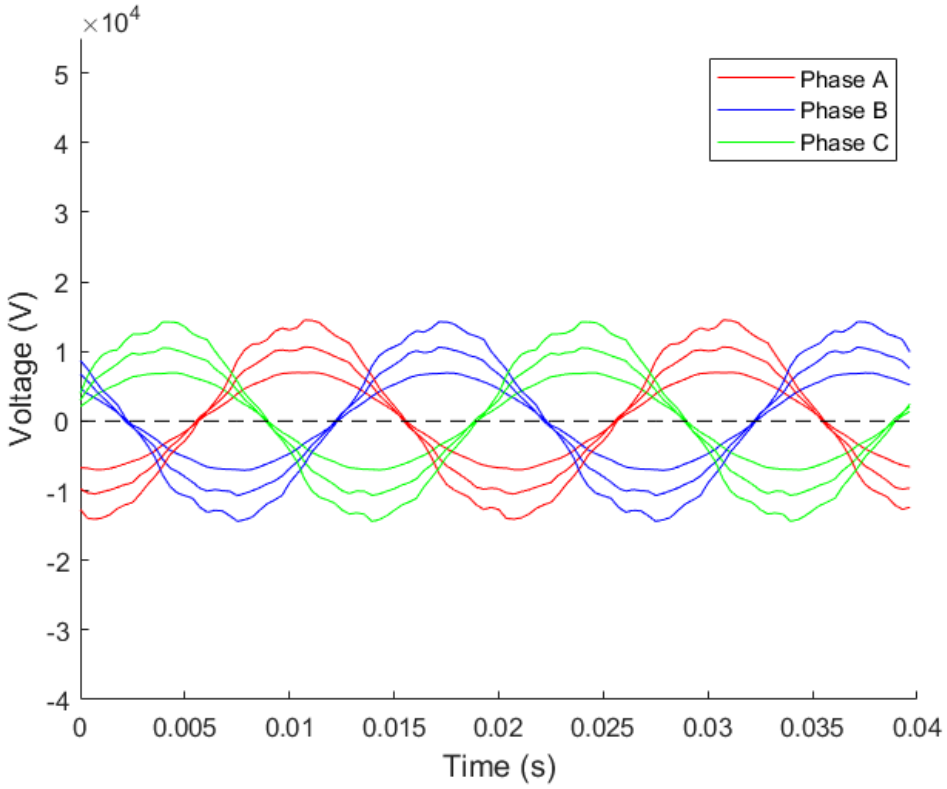

Figure 6.11. *Secondary voltage waveforms of the transformer without air gaps with –10 ° phase shift.*

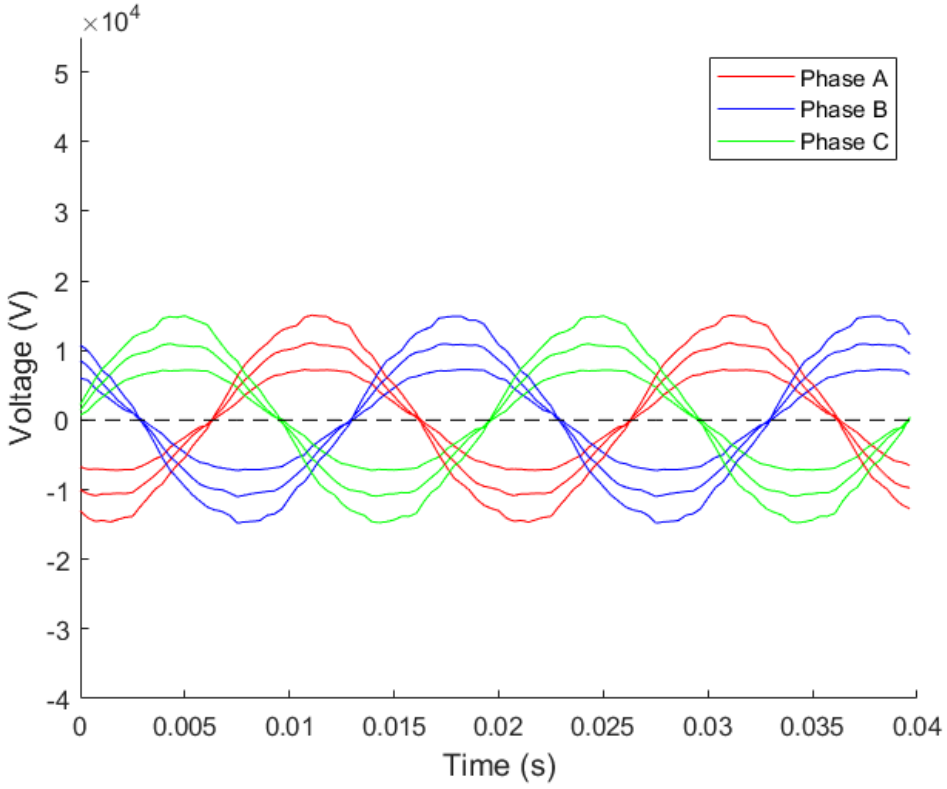

Figure 6.12. *Secondary voltage waveforms of the transformer without air gaps with –20 ° phase shift.*

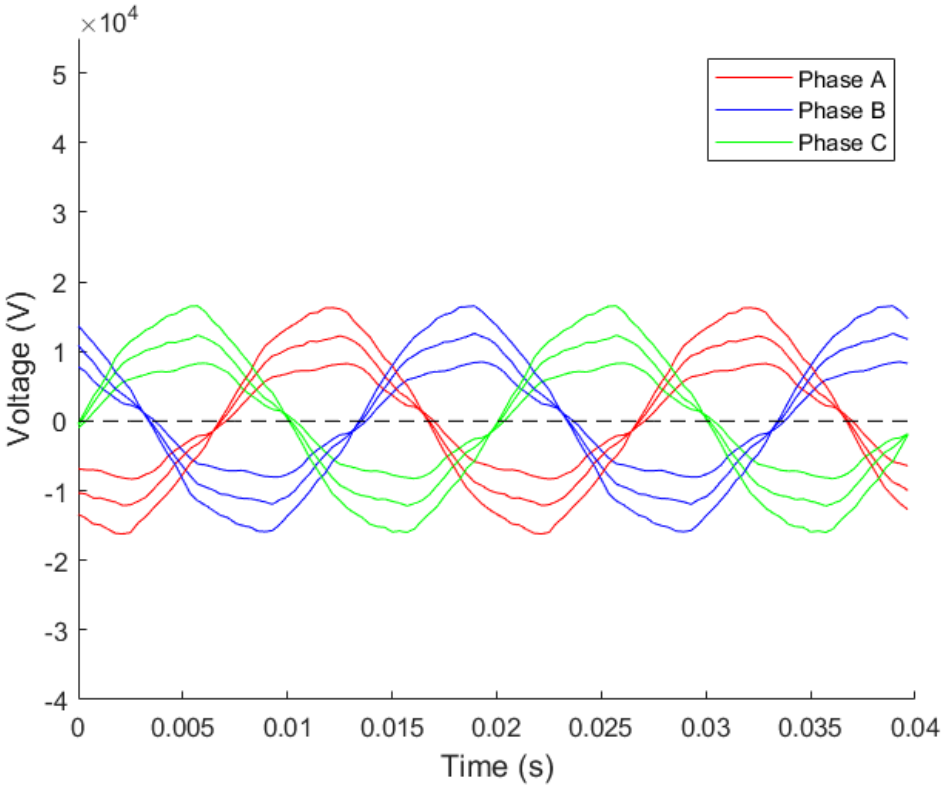

Figure 6.13. *Secondary voltage waveforms of the transformer without air gaps with –30 ° phase shift.*

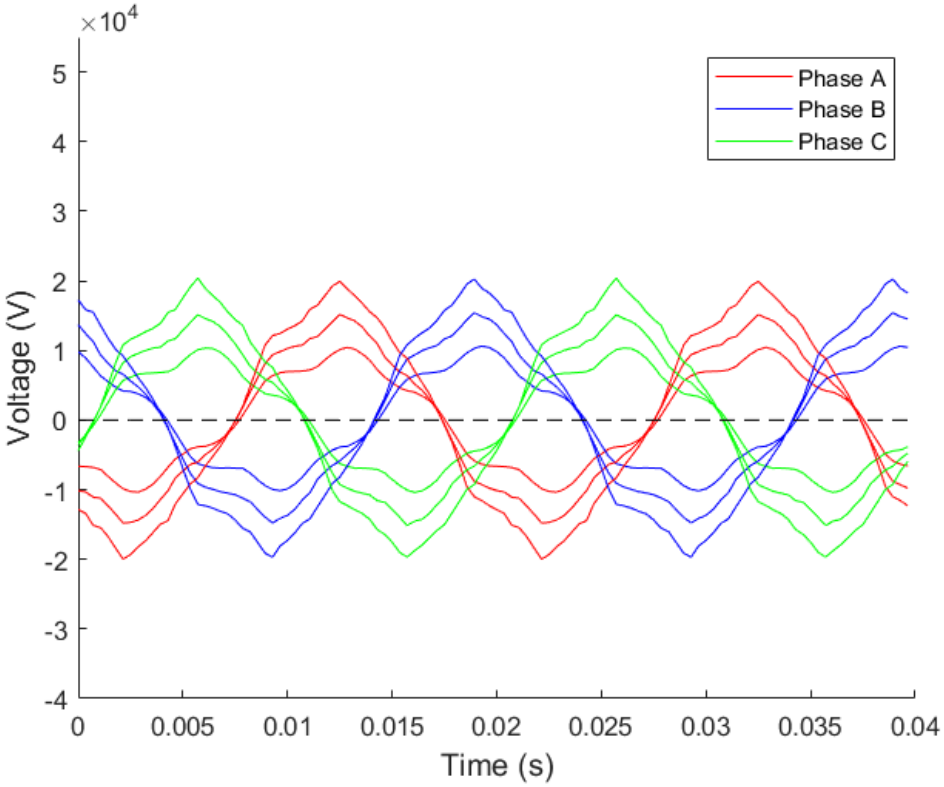

Figure 6.14. *Secondary voltage waveforms of the transformer without air gaps with –40 ° phase shift.*

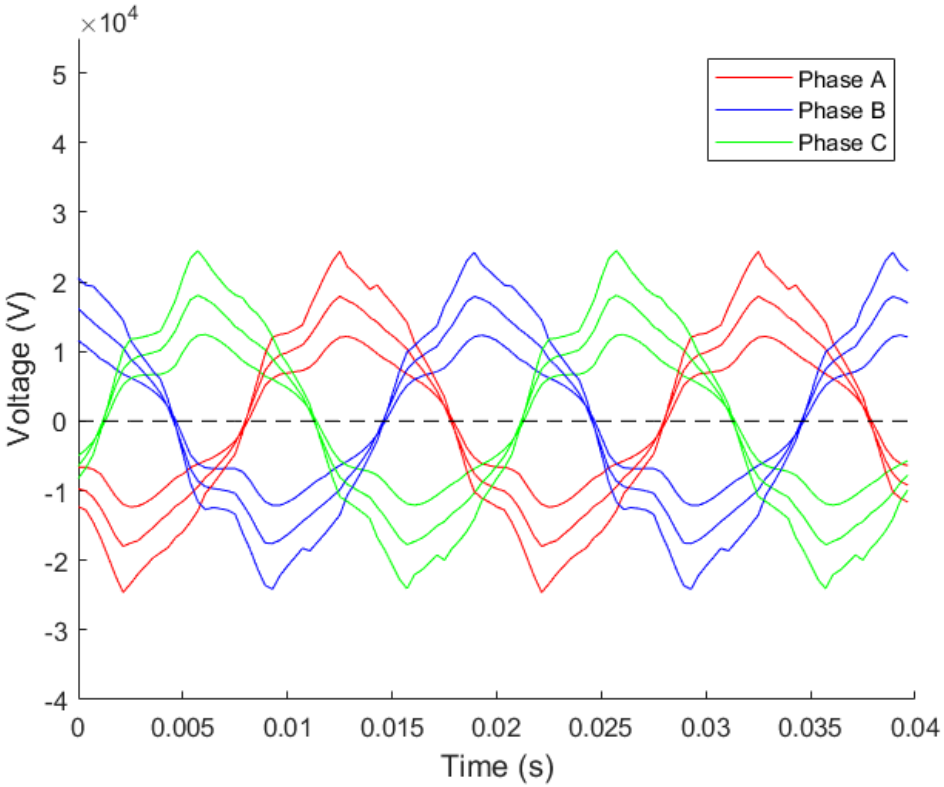

Figure 6.15. *Secondary voltage waveforms of the transformer without air gaps with –50 ° phase shift.*

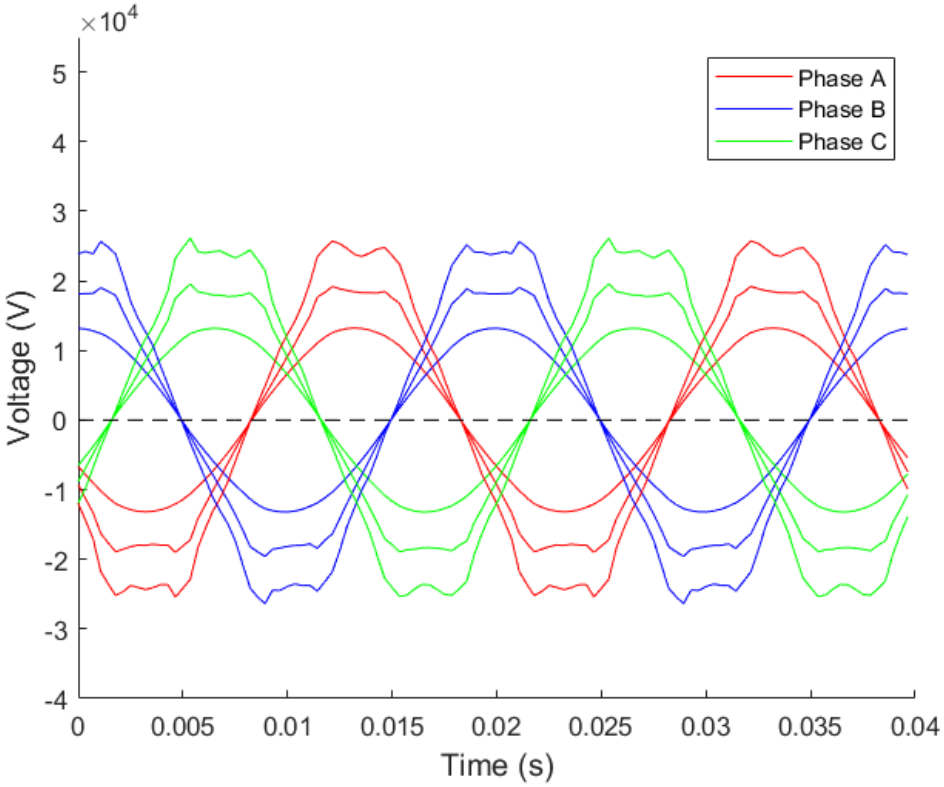

Figure 6.16. *Secondary voltage waveforms of the transformer without air gaps with –59 ° phase shift.*

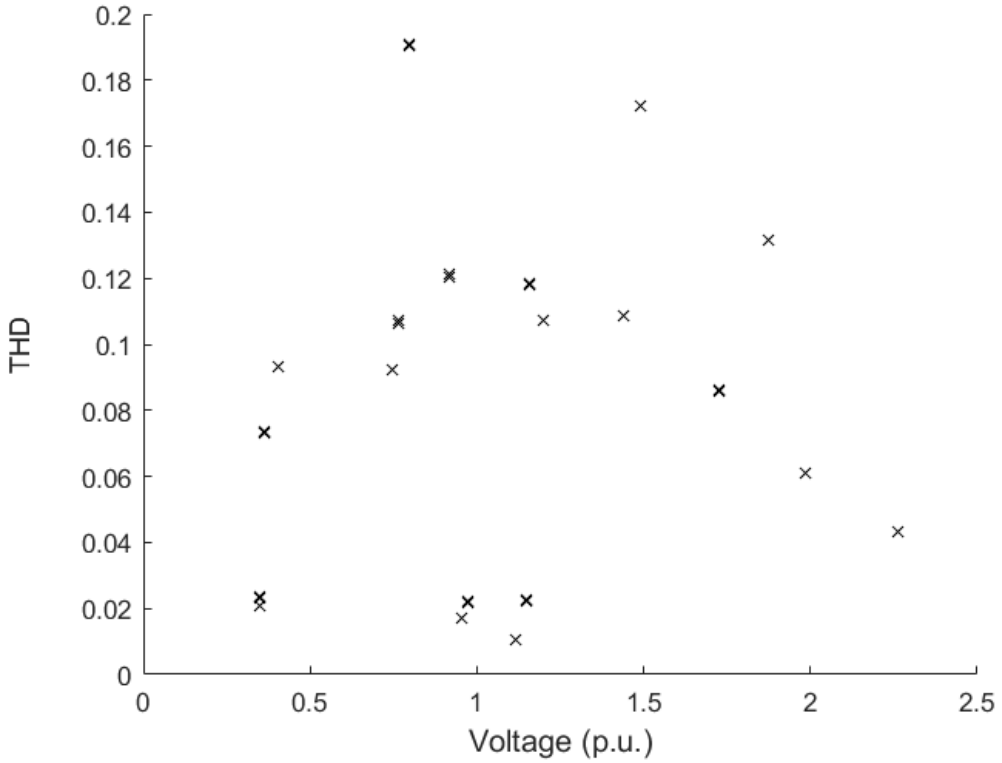

Figure 6.17. *THD vs. secondary voltage of the transformer with the air gaps.*

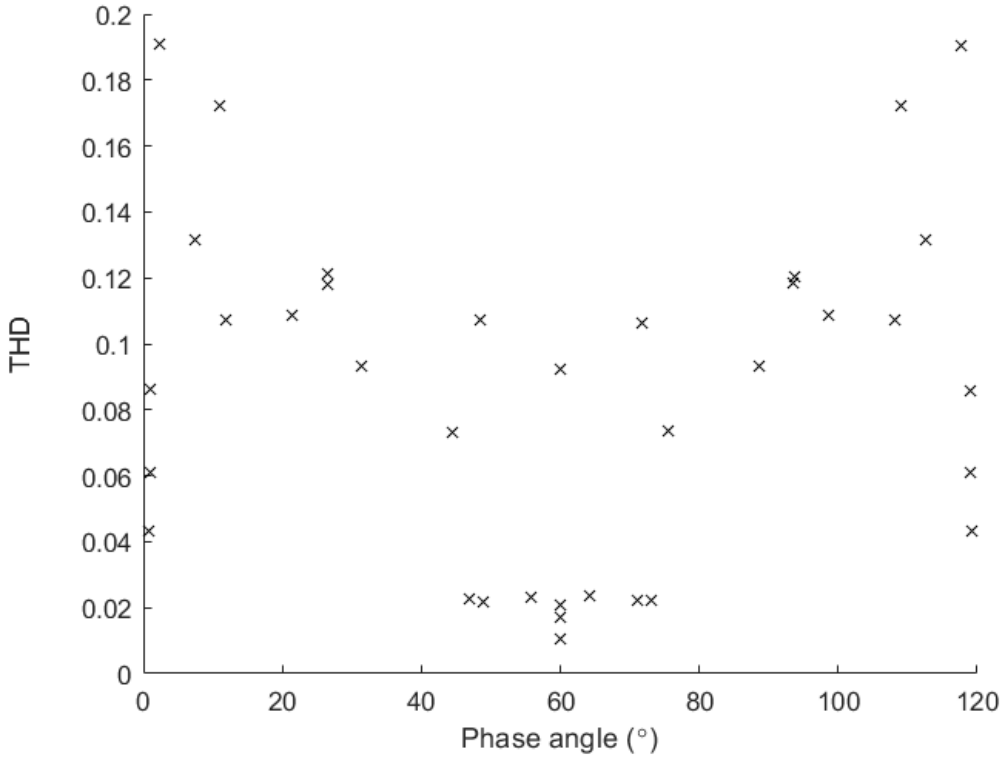

Figure 6.18. *THD vs. phase angle of the secondary side of the transformer with the air gaps.*

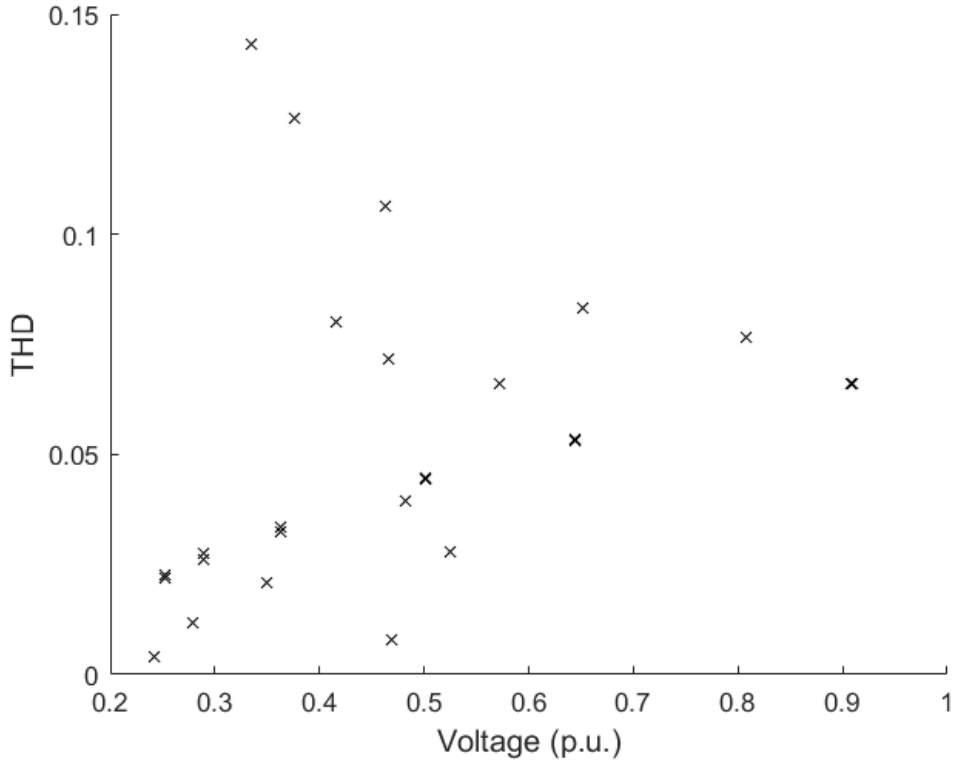

Figure 6.19. *THD vs. secondary voltage of the transformer without the air gaps.*

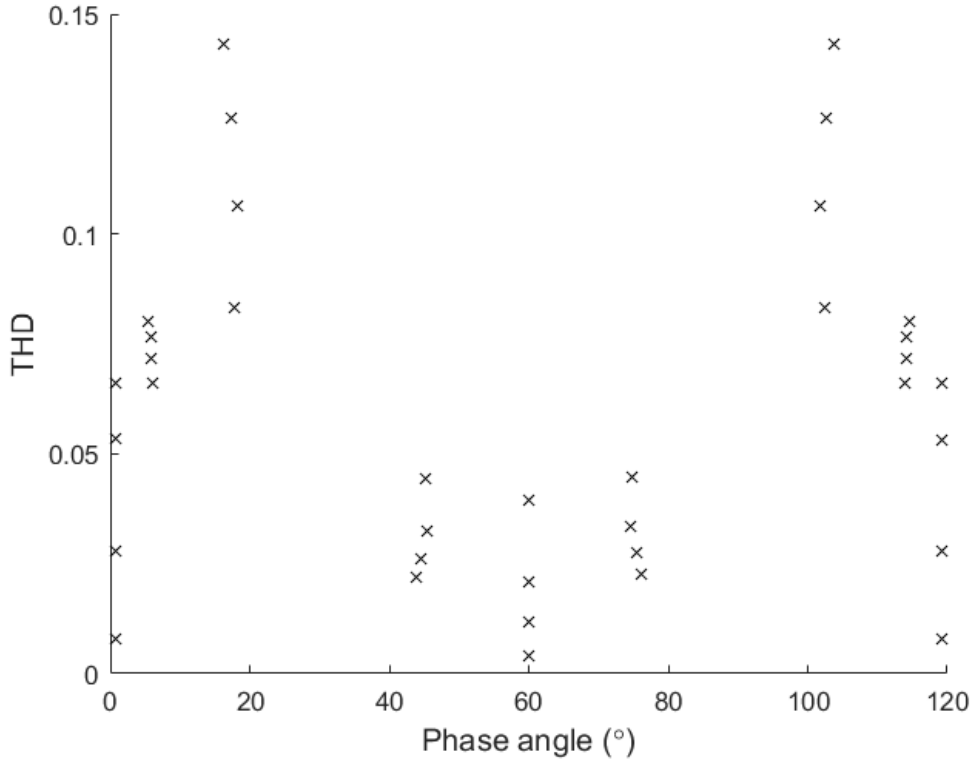

Figure 6.20. *THD vs. phase angle of the secondary side of the transformer without the air gaps.*

The total harmonic distortions (THD) were also calculated for both transformers with and without the air gaps. The THD was calculated for each operating point in Figures 6.2 and 6.1 using

$$\mathrm{THD} = \frac{\sqrt{V_2^2 + V_3^2 + V_4^2 ... + V_n^2}}{V_1} = \frac{\sqrt{V^2 - V_1^2}}{V_1}, \tag{6.6}$$

where V is the root mean square value of the overall voltage and V_i is the root mean square value of the voltage of the harmonic of corresponding order [21]. The results are presented in Figures 6.17–6.20.

As can be seen from Figures 6.17–6.20, the THD seems to be mostly dependent on the phase shift of the transformer. The THD levels are also significantly lower in the transformer with no air gaps, but still higher than what would most likely be considered acceptable. According to a fast Fourier transform analysis, the harmonics in the secondary voltage are mostly of the fifth and seventh order.

7. CONCLUSION

A new design for a variable power transformer, which utilizes its ferromagnetic core for controlling voltage and phase shift, was proposed and analyzed. The transformer was designed for a traditional 50 Hz three-phase power network, as the primary substation transformer with primary voltage of 110 kV, secondary voltage of 20 kV and a power rating of 20 MVA. The transformer consists of three cores with five limbs, which have one primary, four secondary and eight DC biasing coils each.

An analytical model was composed for the transformer, which was then used as basis for the practical design and FEA. It was revealed while analyzing the analytical model that increasing the number of turns in the outermost coils and decreasing the number of turns in the innermost secondary coils expands the operating area of the transformer. This method was used for achieving the theoretical operating area of 0.9–1.1 p.u. secondary voltage and -60–60 ° phase shift with the analytical model.

A practical design and a 2D model for the transformer were composed. Thin air gaps were added in the innermost secondary limbs of the transformer to ensure more even division of the magnetic flux between them and the outermost limbs. The model was then used for FEA of the transformer in no load conditions.

It was revealed through static FEA that the secondary voltage levels of the transformer were too low without thr air gaps in the innermost secondary limbs. It was found through manual testing that 0.5 mm air gaps were enough to bring the secondary voltages up to appropriate levels. An operating area of 0.9–1.1 p.u. secondary voltage and -58–58 ° phase shift was reached, which is very close to the sought-after theoretical operating area.

It was also found through time-stepping FEA that the secondary voltages have increasing harmonic distortion with increasing phase shift. The harmonic distortion was smaller without the air gaps in the innermost secondary limbs, but still significant. The harmonics were mostly of the fifth and seventh order.

Optimization of the transformer with the numbers of turns in the coils and the length of the air gaps as parameters was attempted to maximize the operating area and minimize the harmonic distortion in the secondary voltage. The results however differed only slightly from the initial values, and they weren't therefore presented in this thesis.

The harmonics are a significant problem for the transformer. It's suggested by Dolan and Lehn [17] that the harmonics are introduced to the secondary voltage due to the flux splitting in the core differing with the flux magnitude. In other words, the percentage at which the magnetic flux is divided between the limbs of the core isn't constant throughout the fundamental cycle of the flux. It's also suggested by them that the harmonics could be mitigated through more sophisticated control of the current in the DC biasing coils.

Using air gaps in the innermost secondary limbs of the transformer isn't optimal, and the geometry of the transformer should be changed to eliminate the need for them. This could be achieved with three-dimensional models, e.g. with each of the four secondary limbs in a cross formation around the primary limb, or with a 2D model with each of the three cores separated into two, with voltage and phase shift control on separate cores.

After fixing the issue with the harmonics in the secondary voltage, the transformer should also be simulated in different load conditions. Simulating the transformer with voltage sources on both sides should correspond to a real-life scenario with distributed generation in the distribution network. If the load condition simulations prove successful, the transformer could also be tested in power flow simulations.

REFERENCES

[1] G. Fusco and M. Russo. *Adaptive Voltage Control in Power Systems: Modeling, Design and Applications*. Springer, 2006. 163 pp. URL: https://doi.org/10.1007/978-1-84628-565-3.

[2] J.H. Harlow. *Electric power transformer engineering*. Taylor & Francis, 2012. 613 pp. URL: https://doi.org/10.1201/b12110.

[3] C. Li et al. “Optimal OLTC voltage control scheme to enable high solar penetrations”. In: *Electric power systems research* 160 (2018), p. 318. URL: https://doi.org/10.1016/j.epsr.2018.02.016.

[4] H. Ezzaidi et al. “On the Feasibility of Detecting Faults and Irregularities in On-Load Tap Changers (OLTCs) by Vibroacoustic Signal Analysis”. In: *Sensors (Basel, Switzerland)* 24 (2024), p. 7960. URL: https://doi.org/10.3390/s24247960.

[5] J. Verboomen et al. “Phase shifting transformers: principles and applications”. In: *2005 International Conference on Future Power Systems*. IEEE, 2005. URL: https://doi.org/10.1109/FPS.2005.204302.

[6] Colonel Wm. T. McLyman. *Transformer and inductor design handbook, Fourth Edition.* CRC Press, 2017. 357 pp. URL: https://doi.org/10.1201/b10865.

[7] *IEC Electropedia. Power transformer*. May 25, 2025. URL: https://www.electropedia.org/iev/iev.nsf/display?openform&ievref=421-01-01 (visited on 05/25/2025).

[8] E.V. Larsen. “A classical approach to constructing a power flow controller”. In: *1999 IEEE Power Engineering Society Summer Meeting. Conference Proceedings (Cat. No.99CH36364)*. IEEE, 1999. URL: https://doi.org/10.1109/PESS.1999.787487.

[9] Z. He et al. “A Review of Variable-Inductor-Based Power Converters for Eco-Friendly Applications: Fundamentals, Configurations, and Applications”. In: *Chinese Journal of Electrical Engineering* 9.3 (2023), pp. 50–71. URL: https://doi.org/10.23919/CJEE.2023.000030.

[10] M.S. Perdigao et al. “A variable inductor MATLAB/Simulink behavioral model for application in magnetically-controlled electronic ballasts”. In: *2008 International Symposium on Power Electronics, Electrical Drives, Automation and Motion*. IEEE, 2008. URL: https://doi.org/10.1109/SPEEDHAM.2008.4581201.

[11] L. Zhang, W.G. Hurley, and W.H. Wölfle. “A New Approach to Achieve Maximum Power Point Tracking for PV System With a Variable Inductor”. In: *IEEE transactions on power electronics* 26.4 (2011), pp. 1031–1037. URL: https://doi.org/10.1109/TPEL.2010.2089644.

[12] T. Wass, S. Hornfeldt, and S. Valdemarsson. “Magnetic circuit for a controllable reactor”. In: *IEEE transactions on magnetics* 42.9 (2006), pp. 2196–2200. URL: https://doi.org/10.1109/TMAG.2006.878307.

[13] D. Sevsek et al. “Dynamic Model of a Virtual Air Gap Reactor”. In: *2008 International Symposium on Power Electronics, Electrical Drives, Automation and Motion* 38.4 (2023), pp. 2521–2530. URL: https://doi.org/10.1109/TPWRD.2023.3245123.

[14] S.C. Buitrago, D.B. Cobaleda, and W. Martinez. “Dual Active Bridge Converter with Variable Transformer for Wide Voltage and Wide Load Range Operation”. In: *IEEE access* 11 (2023), pp. 1–1. URL: https://doi.org/10.1109/ACCESS.2023.3308043.

[15] M.S. Perdigao et al. “Magnetically Controlled Electronic Ballasts With Isolated Output: The Variable Transformer Solution”. In: *IEEE transactions on industrial electronics (1982)* 58.9 (2011), pp. 4117–4129. URL: https://doi.org/10.1109/TIE.2010.2102315.

[16] C.S. Buitrago, D.B. Cobaleda, and W. Martinez. “Magnetically Controlled Transformer With Variable Turns Ratio and Low Series Inductance: Analysis and Implementation Toward Its Application in SMPS”. In: *IEEE transactions on power electronics* 38.11 (2023), pp. 14360–14374. URL: https://doi.org/10.1109/TPEL.2023.3300583.

[17] D.S.L. Dolan and P.W. Lehn. “Finite element analysis of a Virtual Air Gap Variable Transformer”. In: *2008 Canadian Conference on Electrical and Computer Engineering*. IEEE, 2008. URL: https://doi.org/10.1109/CCECE.2008.4564664.

[18] V. Molcrette et al. “Reduction of inrush current in single-phase transformer using virtual air gap technique”. In: *IEEE transactions on magnetics* 34 (1998), pp. 1192–1194. URL: https://doi.org/10.1109/20.706479.

[19] F. Zhu and B. Yang. *Power transformer design practices*. CRC Press/Taylor & Francis Group, 2021. 282 pp. URL: https://doi.org/10.1201/9780367816865.

[20] A. Arkkio. “Analysis of Induction Motors Based on the Numerical Solution of the Magnetic Field and Circuit Equations”. PhD thesis. Helsinki University of Technology, 1987. URL: https://urn.fi/urn:nbn:fi:tkk-001267.

[21] *SFS-EN IEC 61000-2-4:2024:en, Electromagnetic compatibility (EMC). Part 2-4: Environment. Compatibility levels in power distribution systems in industrial locations for low frequency conducted disturbances*. 2024.